$d=2$ Ising strip with two surface fields solved using the transfer-matrix method

A. Maciołek and J. Stecki
Institute of Physical Chemistry, Polish Academy of Sciences, Department III, Kasprzaka 44/52, 01-224 Warsaw, Poland
(Received 27 November 1995; revised manuscript received 18 March 1996)

For the title system the column-column transfer matrix is set up and diagonalized by exact calculation. The free energy and correlation length follow exactly from the eigenvalues of the auxiliary problem, whereas other quantities such as magnetization profiles, heat capacities, etc., are calculable numerically with arbitrary accuracy. The case of surface fields with the opposite signs is studied in some detail. The transition from exponentially decaying to oscillatory eigenvectors is discussed and related to wetting transitions. For the important case of the perfect asymmetry system the finite-size scaling near the wetting temperature T_w of surface tension and correlation length parallel to the walls, is derived. Also the scaling of magnetization profiles is found. [S0163-1829(96)09526-4]

I. INTRODUCTION

The exact solutions of the Ising model have proved in the past to be particularly useful in the study of phase transitions.[1–4] A particular formulation of this model refers to a strip of length N and width M. With the emphasis of a strip infinite in one direction $M\to\infty$ it has been studied in the past.[5–7] Since it has been demonstrated that the $d=2$ Ising model can be solved by a transfer-matrix (TM) method in a spinor formulation[7–9] this method has been used with great success in various physical contexts (critical point behavior, surface transition) for a bulk system.[4,9–12]

Of considerable present interest is not a bulk system, but a system confined by walls which may also interact with the neighboring particles (spins) of the system; thus modeling confinement and wetting. However, the added complication of two surface fields, perhaps *opposing* surface fields, has not been solved until now in full generality.

In this work we apply the TM method to study the Ising systems confined between parallel plates or walls. Statistical mechanics of systems in confined geometry has attracted a great deal of interest these last years because of a variety of new phenomena arising in these systems.[13] For a simple fluid, binary mixture or Ising magnet confined between parallel walls, it has been shown that the phase diagram may be severely modified due to the finite distance M between the walls combined with the effects of the surface fields h_1 and h_2 imposed on the boundaries.[5,14–18] In particular, it has been predicted, largely on the basis of Landau theory,[15,16] that the behavior of the Ising magnet strongly depends on whether the fields are of equal or opposite sign, as a consequence of wetting phenomena.

The relevant exact results for a $d=2$ infinitely long Ising strip with the surface fields of *equal* sign imposed on the walls have been obtained using Pfaffians techniques.[5]

In this work we give an exact solution for the column-column transfer matrix taken in the direction *parallel* to the walls to incorporate the effects of the surface fields into the column self-energy from the very start of the calculations. Having found the exact solution of the TM, one finds immediately the free energy, the correlation length, and the surface part of the free energy from which we extract the singular part of the surface tension. Heat capacities follow by numerical differentiation of the free energies. The computation of the magnetization profiles is slightly less immediate, as is described in Sec. V.

We concentrate (Secs. IV and V) on the most interesting case of surface fields of opposite signs. In this context we can introduce a mechanism for breaking the symmetry of the perfectly antisymmetric system. As is well known, the presence of any bulk external field (homogeneous or not) prevents the solution of the Ising model. Therefore the breaking of symmetry with the aid of an external field is not possible but we can instead break the symmetry by making the wall-system interactions different for the two walls. This symmetry-breaking mechanism is spectacularly efficient in the nonwet regime.

The paper is organized as follows. In Sec. II, we define the model, shortly recall the formalism[9,10] and proceed with the solution of the eigenproblem. Reduction of the TM to diagonal form is related to the solution of a certain associated eigenvalue problem. In Sec. III we discuss the solution of the eigenvalue equation, separately for the case of $|h_1|=|h_2|$ and for the case of $|h_1|\neq|h_2|$. In Sec. IV we apply these results and calculate quantities which require only the eigenvalues, such as the surface tension, correlation length, and heat capacities, for the case of surface fields with opposite signs. In Sec. V we derive the formula for the magnetization profiles $m(z)$ and discuss profiles for the system with the surface fields with opposite signs. For the case of the perfect asymmetry system $h_1=-h_2$ we propose and test the scaling law of $m(z)$ in the vicinity of the wetting temperature $T_w(h_1)$. We conclude (Sec. VI) with a summary and a discussion of the results.

II. A TRANSFER-MATRIX SOLUTION FOR $D=2$ ISING MODEL WITH TWO SURFACE LINES OF WEAKENED BONDS

Consider a $d=2$ square lattice in the geometry of infinitely long strip $[N\times(M-1),\ N\to\infty]$ with Ising spins $\sigma(x,z)=\pm1$, $x=1,\ldots,N$, $z=1,\ldots,M-1$ at each lattice site (x,z). The spins are coupled by the Ising Hamiltonian

$$\beta H=-\sum_{z}\sum_{x}\left[K_1\sigma(x,z)\sigma(x+1,z)+K_2\sigma(x,z)\sigma(x,z+1)\right] \tag{2.1}$$

with the cyclic boundary condition along the x axis. $K_i\equiv\beta J_i$, $i=1,2$ are positive coupling constants. We take $K_1=K_2$. To this bulk Hamiltonian the surface term which accounts for the interaction with the walls is added:

$$\beta H_s=-\sum_{x}\left[h_1\sigma(x,1)+h_2\sigma(x,M-1)\right], \tag{2.2}$$

where h_1 and h_2 are the surface fields acting only on the boundary spins.

If $h_i>0(<0)$ then it is said that the wall i favors the $+(-)$ phase. It is convenient for the TM matrix method to replace the surface fields acting on $\sigma(x,1)$ and $\sigma(x,M-1)$, by two rows of modified bonds to additional wall spins $\sigma(x,0)$ and $\sigma(x,M)$, $1\leqslant x\leqslant N$, respectively, with the interaction

$$\sum_{x}\left[a_1K\sigma(x,0)\sigma(x,1)+a_2K\sigma(x,M)\sigma(x,M-1)\right]. \tag{2.3}$$

The bonds are weakened $0\leqslant a_i\leqslant 1$, $i=1,2$ and the spins on additional walls are fixed. This includes four cases. If both $\sigma(x,0)$ and $\sigma(x,M)$ for all x are equal to $+1(-1)$ this is the case of walls which prefer the same $+(-)$ phase. If $\sigma(x,0)=-1(+1)$ but $\sigma(x,M)=1(-1)$ then the walls prefer opposite phases.

The partition function for this model can be expressed as

$$Z_{M,N}=\mathrm{Tr}(T^N), \tag{2.4}$$

where T is the column-column transfer matrix (TM) taken in the x direction and it is known[10] how to take the limit $N\to\infty$ with walls of spins fixed. We take the following symmetrized form of V:

$$T=(2\sinh 2K)^{(M-1)/2}V,$$

$$V=V_2^{1/2}V_1V_2^{1/2}, \tag{2.5}$$

with

$$V_1=\exp\left[-K^*\sum_{1}^{M-1}\sigma_m^z\right], \tag{2.6}$$

$$V_2=\exp[(a_1K)\sigma_0^x\sigma_1^x]\exp\left[K\sum_{2}^{M-1}\sigma_{m-1}^x\sigma_m^x\right]\times\exp[(a_2K)\sigma_{M-1}^x\sigma_M^x], \tag{2.7}$$

where σ^i $(i=x,y,z)$ are the Pauli matrices, $K=\beta J$ and $\tanh K^*=\exp(-2K)$ defines the dual coupling K^*. Note that the presence of two rows of weakened coupling constants breaks the translation symmetry of the problem. The diagonalization of a transfer matrix V, proceeds with the use of Kaufman[8] spinor analysis along the way similar to that described in Ref. 9 for the free boundary condition and Ref. 10 for the fixed $(+/+)$, $(-/-)$ boundary condition. This method uses the fact that the TM operator V written in term of suitable set of spinors is a spin representation of a simple $2(M+1)$ dimensional rotation hence the dimensionality of the eigenvalue problem can be significantly reduced [from 2^{M+1} to $2(M+1)$]. The procedure proceeds in two steps. The first step is to introduce the spinors Γ_k, $k=0,\ldots,2M+1$ by a Jordan-Wigner transformation which is taken here in the standard form:

$$\Gamma_0=\sigma_0^x\quad \Gamma_{2j}=\prod_{0}^{j-1}(-\sigma_m^z\sigma_j^x),$$

$$\Gamma_1=\sigma_0^y\quad \Gamma_{2j+1}=\prod_{0}^{j-1}(-\sigma_m^z\sigma_j^y),$$

$$j=1,\ldots,M.$$

Then the new set of spinors g_k, $k=0,\ldots,2M+1$ is found by an orthogonal transformation $g^T=\Gamma^TS$ such that V in terms of g_k, $k=0,\ldots,2M+1$ is spin representation of a simple $2(M+1)$-dimensional rotations[10]

$$V_g^TV^{-1}=g^TH, \tag{2.8}$$

where

$$H=\begin{pmatrix}1 & & & & \\ & H_1 & & & \\ & & \ddots & & \\ & & & H_M & \\ & & & & 1\end{pmatrix}$$

and

$$H_j=\begin{pmatrix}\cosh\gamma_j & i\sinh\gamma_j\\ -i\sinh\gamma_j & \cosh\gamma_j\end{pmatrix}.$$

Finally g_k, $k=0,2M+1$ are combined in pairs to form the anticommuting Fermi operators $f_k,f_k^\dagger,k=0,\ldots,M$ defined as

$$f_k=(1/2)(g_{2k+1}-ig_{2k}),$$

$$f_k^\dagger=(1/2)(g_{2k+1}+ig_{2k})\quad k=0,\ldots,M.$$

In terms of Fermi operators V has a familiar form

$$V=\exp\left[-(1/2)\sum_{0}^{M}\gamma_k(2f_k^\dagger f_k-I)\right] \tag{2.9}$$

with $\gamma_0=0$. By quantum-mechanical analogy the eigenvectors are ''excited states'' $|L\rangle=f_{l_1}^\dagger\ldots f_{l_j}^\dagger|0\rangle$ with different operators $f_k^\dagger,0<k\leqslant M$ acting on the ''vacuum'' $|0\rangle$ determined by $f_l|0\rangle=0$ for all l. $|L\rangle$ has the eigenvalue

$$\Lambda=\Lambda_0\exp[-\gamma(\omega_{l_1})-\ldots\gamma(\omega_{l_j})], \tag{2.10}$$

where

$$\Lambda_0=\exp\left(\frac{1}{2}\sum_{i=0}^{M}\gamma(\omega_i)\right). \tag{2.11}$$

Each eigenvalue is doubly degenerate and the set $L=(l_1,l_2,l_3,\ldots)$ specifies which γ's enter with a minus sign. To obtain the eigenvectors for the case of surface fields of opposite signs, namely when h_1 prefers the $(-)$ phase but h_2 prefers the $(+)$ phase, we used projection operators[11,12]

$$P_1=(-1/2)(f_0+f_0^\dagger-I), \tag{2.12}$$

$$P_2=(1/2)[(f_0-f_0^\dagger)P+I], \tag{2.13}$$

where P is a parity operator defined as

$$P=\prod_{m=0}^{M}(-\sigma_m^z). \tag{2.14}$$

The excited states $|L\rangle$ are the states with an *odd* number of (different) operators $f_k^\dagger, 0<k\leqslant M$ acting on the vacuum $|0\rangle$. $|L\rangle$ has the eigenvalue of the form (2.10) with the set $L=(l_1,l_2,l_3,\ldots)$ consisting of *odd* elements of different numbers. Since $(\gamma_1<\gamma_2,\ldots)$ the largest eigenvalue is $\lambda_1=\Lambda_0\exp(-\gamma_1)$ and the next is $\lambda_2=\Lambda_0\exp(-\gamma_2)$.

If both walls prefer the same, say $(+)$ phase, the projection operators are

$$P_1=(1/2)(f_0+f_0^\dagger-I), \tag{2.15}$$

$$P_2=(1/2)[(f_0-f_0^\dagger)P+I] \tag{2.16}$$

and the excited states $|L\rangle$ are the states with an *even* number of different operators $f_k^\dagger, 0<k\leqslant M$ acting on the vacuum $|0\rangle$. Now, the largest eigenvalue is $\lambda_1=\Lambda_0$ and the next is $\lambda_2=\Lambda_0\exp(-\gamma_1-\gamma_2)$.

The diagonalization procedure may be reduced to the problem of finding the orthogonal transformation S and the values of γ_k. This can be done by solving the eigenvalue problem for $R\equiv R_2^{1/2}R_1R_2^{1/2}$ where R_1,R_2 are $2(M+1)$-dimensional rotation matrices such that the action of V_1 and V_2 on the set of spinors $\Gamma^T=(\Gamma_0,\ldots,\Gamma_{2M+1})$ is a simple rotation on Γ^T:

$$V_1\Gamma^TV_1^{-1}=\Gamma^TR_1, \tag{2.17}$$

$$V_2\Gamma^TV_2^{-1}=\Gamma^TR_2. \tag{2.18}$$

For the strip with two lines of modified bonds, R_1 and R_2 have the form

$$R_1=\begin{pmatrix} 1 & & & & & & \\ & 1 & & & & & \\ & & A(v_1) & & & & \\ & & & \ddots & & & \\ & & & & A(v_1) & & \\ & & & & & 1 & \\ & & & & & & 1 \end{pmatrix}, \tag{2.19}$$

$$R_2=\begin{pmatrix} 1 & & & & & & \\ & A(v_3) & & & & & \\ & & A(v_2) & & & & \\ & & & \ddots & & & \\ & & & & A(v_2) & & \\ & & & & A(v_4) & & \\ & & & & & 1 & \end{pmatrix}, \tag{2.20}$$

where the matrices $A(v_1)$, $A(v_2)$, $A(v_3)$, and $A(v_4)$ are

$$A(v)=\begin{pmatrix} \cosh v & i\sinh v \\ -i\sinh v & \cosh v \end{pmatrix} \tag{2.21}$$

and $v_1=2K^*$, $v_2=2K$, $v_3=2a_1K$, $v_4=2a_2K$. R is a Hermitian operator so it has the eigenvalues

$$e^{\gamma_0},e^{-\gamma_0},e^{\gamma_1},e^{-\gamma_1},\ldots,e^{\gamma_M},e^{-\gamma_M}$$

with γ_k real with the eigenvectors

$$y_0,y_0^*,y_1,y_1^*,\ldots,y_M,y_M^*$$

that satisfy the normalization condition:

$$y_i^\dagger y_i=\delta_{ij}. \tag{2.22}$$

Having found these eigenvectors one can construct the matrix S

$$S=[\eta_1\xi_1\cdots\eta_M\xi_M] \tag{2.23}$$

with $\xi_i=2^{1/2}(y_i+y_i^*)$ and $\eta_i=2^{1/2}(y_i-y_i^*)$ for $0\leqslant i\leqslant M$. These eigenvectors will be needed for the computation of magnetization profiles.

In the next section the solution of the eigenvalue equation

$$R_2^{1/2}R_1R_2^{1/2}y_m=e^{\gamma(\omega_m)}y_m \tag{2.24}$$

will be described. Such a solution for $a_1=a_2=1$ and $(+/+)$ boundary condition was obtained in Ref. 10, for $a_1=a_2=0$ in Ref. 9 and we have obtained[12] the $(+/-)$ case (for $a_1=a_2=1$) by applying projections to the solution of Ref. 10. Here we find a more general solution for $a_1<1$ and $a_2<1$ with $a_1\neq a_2$ also allowed.

III. THE SOLUTION ON THE EIGENVALUE EQUATION

To solve (2.24) it is convenient to use a modified form of this equation

$$Lx=0 \tag{3.1}$$

with $L=e^{-\gamma}R_1-R_2^{-1}$ and $x=R_2^{1/2}y$. Using expressions for R_1 and R_2 one gets $M-2$ pairs of equations which are the same as for the case of fixed boundary conditions but no weakening of bonds $(a_1=a_2=1)$

$$-ie^{-\gamma}\sinh v_1x_{2n-2}+(e^{-\gamma}\cosh v_1-\cosh v_2)x_{2n-1}+i\sinh v_2x_{2n}=0, \tag{3.2a}$$

$$-i\sinh v_2x_{2n-1}+(e^{-\gamma}\cosh v_1-\cosh v_2)x_{2n}+ie^{-\gamma}\sinh v_2x_{2n+1}=0 \tag{3.2b}$$

for $2\leqslant n\leqslant M-1$.

Besides, the last and the first of the $A(v)$ matrices of R_2 (see 2.20) provide two pairs of equations closing the recurrence (3.2), from above:

$$(e^{-\gamma}-\cosh v_3)x_1+i\sinh v_3x_2=0, \tag{3.3a}$$

$$-i\sinh v_3x_1+(e^{-\gamma}\cosh v_1-\cosh v_3)x_2+(i\sinh v_1)x_3=0 \tag{3.3b}$$

and from below:

$$-ie^{-\gamma}\sinh v_1 x_{2M-2}+(e^{-\gamma}\cosh v_1-\cosh v_4)x_{2M-1}+i\ \sinh v_4 x_{2M}=0, \tag{3.4a}$$

$$-i\ \sinh v_4 x_{2M-1}+(e^{-\gamma}-\cosh v_4)x_{2M}=0. \tag{3.4b}$$

The general solution for x_k, $2\leqslant k\leqslant M-1$ should have the known general form.[9] That is

$$x_{2n}=Bz^{2n}+B'z^{-2n}, \tag{3.5a}$$

$$x_{2n-1}=Az^{2n-1}+A'z^{-2n+1},$$

$$n=2,\ldots,M-1. \tag{3.5b}$$

z is a (complex) number. We note that the coefficients A and B' can be eliminated using the fact that separately $x_{2n}=Bz^{2n}$, $x_{2n-1}=Az^{2n-1}$ and $x_{2n}=B'z^{-2n}$, $x_{2n-1}=A'z^{-2n+1}$ $(n=2,\ldots,M)$ are also solutions of (3.1) if $A/B=-B'/A'\equiv q$ satisfies

$$q=-\frac{e^{-\gamma}\cosh v_1-\cosh v_2}{-i\ \sinh v_2 z^{-1}+ie^{-\gamma}\sinh v_1 z}=-\frac{i\ \sinh v_2 z-ie^{-\gamma}\sinh v_1 z^{-1}}{e^{-\gamma}\cosh v_1-\cosh v_2}. \tag{3.6}$$

This equation has a nontrivial solution if

$$(e^{-\gamma}\cosh v_1-\cosh v_2)^2=z^2(\sinh v_2-e^{-\gamma}\sinh v_1 z^{-2})\times(\sinh v_2 z^{-2}-e^{-\gamma}\sinh v_1). \tag{3.7}$$

From this condition the allowed values of γ_k are related to z. If z is written in the form of $z^2=e^{i\omega}$ with ω complex (3.7) becomes equal to the Onsager function $\gamma(\omega)$:

$$\cosh\gamma=\cosh v_1\cosh v_2-\sinh v_1\sinh v_2\cos\omega. \tag{3.8}$$

The presence of two new constants v_3 and v_4 breaks the symmetry of the matrix L; to satisfy the recurrence (3.2) the solutions for x_1 and for x_{2M} must have coefficients different from the rest of x_{2k} and x_{2k+1} respectively:

$$x_1=Cz+C'z^{-1}, \tag{39a}$$

$$x_M=Dz^{2M}+D'z^{-2M}. \tag{39b}$$

C,C',D,D' can be eliminated from (3.3a) and (3.4b):

$$C=-\frac{i\ \sinh v_3}{e^{-\gamma}-\cosh v_3}\,zB, \tag{3.10}$$

$$C'=-\frac{i\ \sinh v_3}{e^{-\gamma}-\cosh v_3}\,z^{-1}B', \tag{3.11}$$

$$D=-\frac{i\ \sinh v_4}{e^{-\gamma}-\cosh v_4}\,z^{-1}A, \tag{3.12}$$

$$D'=-\frac{i\ \sinh v_4}{e^{-\gamma}-\cosh v_4}\,zA'. \tag{3.13}$$

Now, the general solution is written in terms of only two coefficients B and A'

$$x_1=-\left(\frac{i\ \sinh v_3}{e^{-\gamma}-\cosh v_3}\right)B[z^2-(A'/B)qz^{-2}],$$

$$x_{2n}=B[z^{2n}-(A'/B)qz^{-2n}],$$

$$x_{2n+1}=B[qz^{2n+1}+(A'/B)z^{-(2n+1)}],$$

$$x_{2M}=\left(\frac{i\ \sinh v_4}{e^{-\gamma}-\cosh v_4}\right)B[qz^{2M-1}+(A'/B)'z^{-2M+1}]$$

$$1\leqslant j\leqslant M-1. \tag{3.14}$$

A'/B has to be determined from the boundary conditions of the recurrence (3.2). (3.3b) and (3.4a) give

$$\frac{B}{A'}=z^{-5}\,\frac{T_1qz-ie^{-\gamma}\sinh v_1}{T_1+ie^{-\gamma}\sinh v_1 qz}, \tag{3.15a}$$

$$\frac{B}{A'}=-z^{-4M+3}\,\frac{T_2+ie^{-\gamma}\sinh v_1 qz}{T_2qz-ie^{-\gamma}\sinh v_1}, \tag{3.15b}$$

where

$$T_{1,2}=\frac{-\sinh^2 v_{3,4}}{e^{-\gamma}-\cosh v_{3,4}}+(e^{-\gamma}\cosh v_2-\cosh v_{3,4}). \tag{3.16}$$

In conclusion, (3.14) is a solution of (3.1) with

$$\frac{B}{A'}=z^{-5}\,\frac{T_1qz-ie^{-\gamma}\sinh v_1}{T_1+ie^{-\gamma}\sinh v_1 qz},$$

provided (3.7) is obeyed and z satisfies the eigenvalue equation

$$(z^2)^{2(M-2)}=\left[\frac{T_1+ie^{-\gamma}\sinh v_1 qz}{T_1qz-ie^{-\gamma}\sinh v_1}\right]\left[\frac{T_2+ie^{-\gamma}\sinh v_1 qz}{T_2qz-ie^{-\gamma}\sinh v_1}\right]. \tag{3.17}$$

Then the eigenvectors y are given by $y=R_2^{-1/2}x$ so after some algebra we obtain

$$y_1=-iB_1\mathcal{A}(v_3)\left[\sinh\frac{v_2}{2}\,[z^2e^{i\delta^*}+z^4R(z)]+\cosh\frac{v_2}{2}\,[z^2+z^4R(z)e^{i\delta^*}]\right], \tag{3.18a}$$

$$y_2=B_1\mathcal{B}(v_3)\left[\sinh\frac{v_2}{2}\,[z^2e^{i\delta^*}+z^4R(z)]+\cosh\frac{v_2}{2}\,[z^2+z^4R(z)e^{i\delta^*}]\right], \tag{3.18b}$$

$$y_{2n+1}=iB_1[z^{2n+2}e^{i\delta^*}+z^{-2n+4}R(z)], \tag{3.18c}$$

$$y_{2n+2}=B_1[z^{2n+2}+z^{-2n+4}R(z)e^{i\delta^*}], \tag{3.18d}$$

$$y_{2M-1}=iB_1\mathcal{A}(v_4)\Big[\cosh\frac{v_2}{2}\,[z^{2M}e^{i\delta^*}+z^{-2M+6}R(z)]+\sinh\frac{v_2}{2}\,[z^{2M}+z^{-2M+6}R(z)e^{i\delta^*}]\Big], \tag{3.18e}$$

$$y_{2M}=-B_1\mathcal{B}(v_4)\Big[\sinh\frac{v_2}{2}\,[z^{2M}e^{i\delta^*}+z^{-2M+6}R(z)]+\cosh\frac{v_2}{2}\,[z^{2M}+z^{-2M+6}R(z)e^{i\delta^*}]\Big], \tag{3.18f}$$

$$y_0=0,$$

$$y_{2M+1}=0,$$

where

$$\mathcal{A}(v_i)=[\cosh v_i/2\ \sinh v_i/(e^{-\gamma}-\cosh v_i)+\sinh v_i/2], \tag{3.19a}$$

$$\mathcal{B}(v_i)=[\sinh v_i/2\ \sinh v_i/(e^{-\gamma}-\cosh v_i)+\cosh v_i/2], \tag{3.19b}$$

where $i=3,4$ and

$$R(z)\equiv -i\,\frac{T_1+ie^{-\gamma}\sinh v_1 qz}{T_1 qz-ie^{-\gamma}\sinh v_1}. \tag{3.20}$$

Also

$$e^{i\delta^*(\omega)}=(B/A)^{1/2}\left[\frac{(z^2-A)(z^2-B^{-1})}{(z^2-A^{-1})(z^2-B)}\right]^{1/2} \tag{3.21}$$

with $A^{-1}=\tanh K\tanh K^*$, $B=\tanh K/\tanh K^*$ and the branch of the square root is taken such that $\exp\delta^*(0)=+1$. The function $\delta^*(\omega)$ is introduced in the above derivation through the following identity:

$$q=iz\,\frac{e^{i\delta^*}\cosh v_2/2+\sinh v_2/2}{e^{i\delta^*}\sinh v_2/2+\cosh v_2/2}. \tag{3.22}$$

$\delta^*(\omega)$ and γ_k which appear naturally here, are the parameters of the Onsager hyperbolic triangle[24] defined by (3.8) and the set of equations:

$$(\sinh\gamma)\cos\delta'=\sinh v_1\cosh v_2-\cosh v_1\sinh v_2\cos\omega, \tag{3.23}$$

$$(\sinh\gamma)\cos\delta^*=\cosh v_1\sinh v_2-\sinh v_1\cosh v_2\cos\omega, \tag{3.24}$$

$$\frac{\sin\delta'}{\sinh v_2}=\frac{\sin\delta^*}{\sinh v_1}=\frac{\sin\omega}{\sinh\gamma}. \tag{3.25}$$

The constant B_1 is determined from the normalization condition (2.22).

The last step of the diagonalization procedure is an examination of Eq. (3.17). This equation determines the allowed values of the ω_k and from (3.8) also of γ_k. We start the discussion of a possible solutions with the simplification of the right-hand side (rhs) of this equation. As can be shown after considerable algebra $R(z)$ may be written as

$$R(z)=-e^{i\delta'}\,\frac{W_1(z^2-W_1^{-1})}{z^2(z^2-W_1)}, \tag{3.26}$$

where

$$W_1=(\cosh v_1+1)(\cosh v_2-\cosh v_3). \tag{3.27}$$

Above $\delta'(\omega)$ is a parameter of Onsager's hyperbolic triangle defined by (3.23) and (3.25) with the following factor form:

$$e^{i\delta'(\omega)}=(AB)^{-1/2}\left[\frac{(z^2-A)(z^2-B)}{(z^2-A^{-1})(z^2-B^{-1})}\right]^{1/2}, \tag{3.28}$$

such that $\exp i\delta'(0)=-1$. W_1 is just the same temperature function as was used to define the wetting temperature $T_w(h_1), h_1=a_1J\sigma_0$, in the semi-infinite Ising model with a single surface field h_1.[19] At $T=T_w(h_1)W_1$ is equal to 1. If $T<T_w(h_1)$ then $W_1>1$. Using (3.26) Eq. (3.17) can be written as

$$(z^2)^{2M}=e^{2i\delta'}\left(\frac{W_1z^2(z^2-W_1^{-1})}{z^2-W_1}\right)\left(\frac{W_2z^2(z^2-W_2^{-1})}{z^2-W_2}\right), \tag{3.29}$$

where

$$W_2=(\cosh v_1+1)(\cosh v_2-\cosh v_4) \tag{3.30}$$

defines the wetting temperature $T_w(h_2), h_2=a_2J\sigma_M$, in the semi-infinite system with a single surface field h_2. We look for the roots of the ''eigenvalue'' equation taking $z^2=e^{i\omega}$ with ω real, between 0 and π and check if they give rise the appropriate number of the eigenvectors. The cases of (a) $|h_1|=|h_2|$ and (b) $|h_1|\neq|h_2|$ are discussed separately.

A. The case of $|h_1|=|h_2|$

For this case $W_1=W_2\equiv W$ and (3.29) simplifies considerably

$$e^{i\omega M}=\alpha e^{i\delta'}\,\frac{We^{i\omega}(e^{i\omega}-W^{-1})}{e^{i\omega}-W} \tag{3.31}$$

with $\alpha=\pm1$. For ω real we define

$$e^{i\phi}=\frac{We^{i\omega}(e^{i\omega}-W^{-1})}{e^{i\omega}-W}, \tag{3.32}$$

where $\phi(\omega)$ is a real function so that the allowed wave numbers ω_k between 0 and π could be find graphically or numerically by rewriting the (3.31) in the form

$$\tan M\omega=\tan(\delta'+\phi)(\omega), \tag{3.33}$$

$$(\delta'+\phi)(\omega)=M\omega-(k-1)\pi. \tag{3.34}$$

As is well known,[9,10] $\delta'(\omega)$ has a different ω dependence below and above $T_{c,\infty}$, the critical temperature of the infinite system. A detailed examination of $\phi(\omega)$ shows that this function changes its behavior not only at $T_{c,\infty}$ but also at $T_w(h_1)$—the wetting temperature of the semi-infinite system. Thus we distinguish three temperature regions: (1) $T<T_w(h_1)$, (2) $T_w(h_1)\leqslant T<T_{c,\infty}$, and (3) $T_{c,\infty}<T$.

At $T=T_w(h_1)$ there is a special solution at $\omega=0$ with nonzero eigenvector and the corresponding eigenvalue $e^{\gamma(0)}=e^{v_2-v_1}$. For all other temperatures the values $\omega=0,\pi$ give the trivial eigenvectors.

The results for ω_k, and γ_k, $k=1,\ldots,M$ are as follows.

(1) $T<T_w(h_1)$.

Below $T_w(h_1)$ there are $M-2$ real solutions between 0 and π. $\gamma_k\equiv\gamma(\omega_k)$ are given by (3.8) and they are all greater than $v_0\equiv v_2-v_1$. Two ''missing'' solutions are found at imaginary value $\omega_1=iu_1$ and $\omega_2=iu_2$, $u_{1,2}\geqslant 0$ from

$$e^{-u_k M}=\alpha_k e^{i\delta'(iu_k)}\,\frac{We^{-u_k}(e^{-u_k}-W^{-1})}{e^{-u_k}-W}, \qquad (3.35)$$

where $k=1,2$ and $\alpha_1=1,\alpha_2=-1$. The solutions lie between B^{-1} and 1 near W^{-1}. In the limit $M\to\infty$ they become equal to $e^{-u_1}=e^{-u_2}=W^{-1}$. For large but finite M, the difference $u_{1,2}-u_0$, where $u_0\equiv\ln W$, is exponentially small

$$u_k-u_0\sim-\alpha_k 2e^{-u_0 M}e^{-i\delta'(iu_0)}\sinh u_0 e^{u_0}, \qquad (3.36)$$

$k=1,2$.

Having found $u_{1,2}$, γ_i, $i=1,2$ are calculated from

$$\cosh\gamma_i=\cosh v_0+1-\cosh u_i, \quad i=1,2, \qquad (3.37)$$

$u_1>u_2$ hence $\gamma_1<\gamma_2<v_0$. With the increasing temperature W^{-1} goes to 1 and at $T_{w,M}(h_1)$ that lies slightly below $T_w(h_1)$ the imaginary solution u_2 disappears. At the same time a real solution near $\omega=0$ appears. $T_{w,M}$ is determined from

$$M=1/(\sinh v_1/\tanh v_2-\cosh v_1)+2(1-W)/(2-W-W^{-1}). \qquad (3.38)$$

For large M and not too small a_1, $T_{w,M}(h_1)\sim T_w(h_1)-C_1(h_1)/M$. Thus between $T_{w,M}(h_1)$ and $T_w(h_1)$ there are $M-1$ real solutions ω_k with $\gamma_k>v_0$ and one imaginary solution $\omega_1=u_1$ with $\gamma_1<v_0$.

(2) $T_w(h_1)\leqslant T<T_{c,\infty}$.

At $T_w(h_1)$ all ω_k become real with $\omega_1=0$ and $\gamma_1=\gamma(\omega=0)$, the smallest of γ's becomes *equal to* v_0. All solutions ω_k remain real up to the temperature $T_{c,M}$ that lies slightly above $T_{c,\infty}$. $T_{c,M}$ is given also by (3.38) but solved above $T_{c,\infty}$. For large M, $T_{c,M}(h_1)\sim T_{c,\infty}-C_2(h_1)/M$. All γ_k are greater than v_0.

(3) $T>T_{c,\infty}$.

Above $T_{c,M}$ there appears again one imaginary solution $\omega_1=iu$ and $M-1$ real. u is found between B and 1 from (3.35) with $\alpha_1=1$.

B. The case of $|h_1|\neq|h_2|$

We take $|h_1|<|h_2|$ so that $T_w(h_1)>T_w(h_2)$. The real solutions between 0 and π which give rise to nontrivial eigenvectors are found from

$$\tan M\omega=\tan\left[\delta'(\omega)+\frac{\phi_1+\phi_2(\omega)}{2}\right], \qquad (3.39)$$

where $\phi_{1,2}$ are defined by (3.32) with $W=W_{1,2}$, respectively. Now, there are three characteristic temperatures in the system: the wetting temperatures for walls $T_w(h_1)$, $T_w(h_2)$, and $T_{c,\infty}$. The examination of $\phi_{1,2}$ shows that in this case where there is no perfect asymmetry in a system we have to distinguish four temperature regions: (1) $T<T_w(h_2)$, (2) $T_w(h_2)<T<T_w(h_1)$, (3) $T_w(h_1)<T<T_{c,\infty}$, and (4) $T_{c,\infty}<T$.

The results for the allowed number of ω_k and γ_k are as follows.

(1) $T<T_w(h_2)<T_w(h_1)$.

Below $T_w(h_2)$, which is the lower of the two, there are $M-2$ real solutions for ω between 0 and π—just as in case (a) below the wetting temperature $T_w(h_1)=T_w(h_2)$. The missing two roots are found from (3.29) for $z^2=e^{i\omega}$ and $\omega=iu$ between B^{-1} and 1 close to the W_1^{-1} and W_2^{-1} [which are zeros of the rhs of (3.29)]. For $T_w(h_1)>T_w(h_2)$, $W_1^{-1}<W_2^{-1}$, so that u_1 lies exponentially close to $u_{01}\equiv\ln W_1$ and u_2 lies exponentially close to $u_{02}\equiv\ln W_2$:

$$u_1-u_{01}\sim-2\sinh u_{01}e^{-2Mu_{01}}e^{-2i\delta'(iu_{01})}\times(1-W_2W_1)/(W_2W_1^{-1}-1), \qquad (3.40)$$

$$u_2-u_{02}\sim 2\sinh u_{02}e^{-2Mu_{02}}e^{-2i\delta'(iu_{02})}\times(1-W_1W_2)/(W_1W_2^{-1}-1). \qquad (3.41)$$

$u_1>u_2$ hence $\gamma_1<\gamma_2<u_0$.

(2) $T_w(h_2)<T<T_w(h_1)$.

In this temperature region there are $M-1$ real solutions and one imaginary $\omega_1=iu_1$ with $\gamma_1<v_0$. The imaginary solution that lies close to W_2^{-1} disappears—not exactly at $T_w(h_2)$ but at $T_{w,M}(h_2)$ which is slightly below $T_w(h_2)$.

(3) $T_w(h_1)<T<T_{c,\infty}$.

In this region all roots become real and all γ_k are greater than v_0. The imaginary solution that lies close to W_1^{-1} disappears, not exactly at $T_w(h_1)$ but at $T_{w,M}(h_1)$ slightly below $T_w(h_1)$.

Both $T_{w,M}(h_2)$ and $T_{w,M}(h_1)$ are given by the roots of

$$M=1/(\sinh v_1/\tanh v_2-\cosh v_1)+\frac{(1-W_1)}{(2-W_1-W_1^{-1})}+\frac{(1-W_2)}{(2-W_2-W_2^{-1})}. \qquad (3.42)$$

(4) $T_{c,\infty}<T$.

Just as in the case of perfect asymmetry, there are $(M-1)$ real solutions above $T_{c,M}$. $T_{c,M}$ is a third root of (3.42) which lies above $T_{c,\infty}$. The imaginary ω is found from (3.29) between B and 1. The mechanism of breaking the symmetry of the perfectly asymmetric system with $|h_1|=|h_2|$ is further discussed below.

The above discussion is of a great importance for the form of the eigenvectors y_k (3.18). As the exact expressions (3.18) for y_k, $k=1,\ldots,2M$ show, real ω corresponds to oscillatory behavior of the eigenvectors whereas the (one or two) missing roots with purely imaginary ω correspond to exponentially decaying eigenvectors. Such exponential decay is needed to describe the fast fall of magnetization and other properties near either wall—hence below the wetting temperature in the nonwet regime but also above $T_{c,\infty}$ where at

sufficiently high temperatures the system is filled with disordered bulk phase—except for a few layers of adsorbed matter at a wall.

IV. ISING STRIP WITH THE SURFACE FIELDS OF THE OPPOSITE SIGNS

The results obtained in the previous sections are now applied to the case when the surface fields h_1, h_2 have the opposite signs. We fix spins $\sigma(x,0)$, $x=1,\ldots,N$ at the value -1 and $\sigma(x,M)$, $x=1,\ldots,N$ at the value $+1$ so that $h_1<0$ and $h_2>0$. We calculate the surface tension (surface excess free energy per unit area) from the definition [4]

$$\beta\sigma(M)=-\lim_{N\to\infty}\ln\frac{Z^{-+}}{Z^{++}}, \tag{4.1}$$

where Z^{-+} is a partition function for the system with the surface fields of opposite signs and Z^{++} is a partition function for the similar system but with the surface fields of equal signs [$\sigma(x,0)$ and $\sigma(x,M)$ fixed at the value $+1$ for all $x=1,\ldots,N$].

In the limit $N\to\infty$ it is enough to know the highest eigenvalue of the TM. For the $(+/+)$ case it is Λ_0 given by (2.10), for the $(-/+)$ case it is $\Lambda_0 e^{-\gamma_1}$, thus

$$\beta\sigma=\gamma_1. \tag{4.2}$$

We also consider the correlation length $\xi_\parallel$ in a direction parallel to the wall, which is defined through the spectral gap between the two highest eigenvalues

$$\xi_\parallel^{-1}=[\ln(\lambda_1/\lambda_2)]^{-1}=(\gamma_2-\gamma_1). \tag{4.3}$$

Having the expressions for γ_1 and γ_2 in the various temperature regions the discussion of the asymptotic behavior and scaling for the surface tension $\sigma(M)$ and longitudinal correlation length $\xi_\parallel$ is straightforward.

A. The case of the perfect asymmetry $h_1=-h_2$

Below the wetting temperature $T_w(h_1)$ γ_1 is given by (3.8) with the imaginary wave number $\omega_1=iu_1$ and is less than $v_0\equiv v_2-v_1$. Hence, as can be expected for the nonwet region, the surface tension of the interface bound to the $(-)$ or $(+)$ wall is less than $\beta^{-1}v_0$—the Onsager surface tension for the free interface in the Ising system.

An asymptotic behavior of γ_1 for large distance M between the walls and for the temperature fixed at any value below $T_w(h_1)$, can be derived from (3.37) and (3.36). For large M, γ_1 is exponentially close to the γ_0 given by

$$\cosh\gamma_0=\sinh v_0+1-\cosh u_0, \tag{4.4}$$

where $u_0=\ln W$.

$$\gamma_1=\gamma_0-C(T,h_1)e^{-Mu_0} \tag{4.5}$$

with $C(T,h_1)=2(e^{u_0}\sinh^2 u_0/\sinh\gamma_0)\exp[-i\delta'(iu_0)]$.

$(1/\beta)\gamma_0$ is the surface tension of the interface below $T_w(h_1)$ (bound to the wall) obtained exactly by Abraham in the semi-infinite Ising model for the wetting transition.[19] This surface tension exhibits a jump in the second temperature derivative at the wetting temperature. In a strip of finite width this discontinuity is rounded and in the vicinity of $T_w(h_1)$ we consider a finite-size scaling. The small parameter which measures the distance to the wetting temperature is u_0. It is equal to 0 at $T_w(h_1)$. The bulk (semi-infinite) system is wet for $u_0<0$ and nonwet for the $u_0>0$. The scaling limit is defined as $u_0\to 0$, $n\equiv M-1\to\infty$ but $X\equiv nu_0=O(1)$. $n\equiv M-1$ is the width of the strip where only the active spins are taken into account. As $u_0\to 0$ than $\gamma_1\to v_0$ and the lhs of Eq. (3.36) can be expanded around v_0. The rhs of this equation is expanded around $u_0=0$ using (3.35). In the scaling limit we get

$$\gamma_1=v_0=-(1/4\,\sinh v_0)u_0^2(1-2e^{-X})^2+O(u_0^3) \tag{4.6}$$

and the scaling for the singular part of the surface tension in the vicinity of the wetting temperature has the form

$$\beta\sigma_s\equiv\gamma_1-v_0=-n^{-2}F(X) \tag{4.7}$$

with the scaling function $F(X)=(1/4\,\sinh v_0)X^2(1-2e^{-X})^2$. In the limit $X\to\infty$, corresponding to the nonwet region $u_0\gg n^{-1}$, $F(X)\sim X^2$. In this limit the behavior of the bulk critical wetting is recovered.[19] The opposite limit cannot be taken because the above derivation is valid only for $T<T_w(h_1)$, where ω_1 is a pure imaginary number.

At $T_w(h_1)$ the surface tension $\sigma(M)\equiv(1/\beta)\gamma_1$ becomes equal to $(1/\beta)v_0$—the surface tension of the free interface. Above $T_w(h_1)$, $\beta\sigma(M)$ remains, up to the finite-size corrections, equal to v_0. These corrections are calculated from (3.8) using the fact that in the wet region ω_1 is a real root of (3.33) between 0 and π/M. For large M, $\omega_1\to 0$ and $\gamma_1\to v_0$. If the wetting temperature is well below $T_{c,\infty}$ so that v_0 is not a small parameter, the finite-size behavior of γ_1 can be obtained by expanding (3.33) and (3.8) about $\omega=0$. For $M\to\infty$ at constant T

$$\omega_1=\pi M^{-1}+(A_1+B_1)\pi M^{-2}+\cdots, \tag{4.8}$$

where $A_1=1/(\sinh v_1/\tanh v_2-\cosh v_1)$ and $B_1=(1-\cosh u_0+\sinh u_0)/(1-\cosh u_0)$. It follows from (3.8) that

$$\beta\sigma(M)=v_0+(1/2\beta\Gamma)\pi^2M^{-2}+O(M^{-3}), \tag{4.9}$$

where the stiffness of the interface $\beta\Gamma=\sinh v_0$. This is a well-known result[20,21,23] for the finite-size effects in the surface tension of the planar fluctuating interface in the Ising model. For the case $a_1=a_2=1$ see Ref. 23.

Close to the critical temperature $T_{c,\infty}$ the singular part of the surface tension should obey the standard finite-size scaling. The scaling limit is now $M\to\infty$, $t\equiv(T-T_{c,\infty})/T_{c,\infty}\to 0$ but $X\equiv Mt=O(1)$. As $t\to 0$, $v_0\to 0$. In this limit the equation for ω_k (3.33) takes the form

$$\tan(M\omega_1)=\frac{\omega_k}{-v_0} \tag{4.10}$$

and the further derivation of the scaling function for the singular part of the surface tension is the same as has been done previously for the case of the Ising strip with fixed $(-/+)$ boundary condition for $(a_1=a_2=1)$.[22,23]

For the correlation length $\xi_\parallel$ both γ_1 and γ_2 are needed. As the finite-size dependence of γ_1 and γ_2 is different below and above $T_w(h_1)$ there is a qualitatively different behavior of $\xi_\parallel$ in these two regions.

In the nonwet region [below $T_{w,M}(h_1)$] both γ's come from imaginary wave numbers $\omega_1=iu_1$ and $\omega_2=iu_2$. For large M, γ_1 is given by (4.5) and γ_2 takes the following form:

$$\gamma_2=\gamma_0+C(T,h_1)e^{-Mu_0}, \tag{4.11}$$

where γ_0 is given by (4.4), $C(T,h_1)=2(e^{u_0}\sinh^2 u_0/\sinh\gamma_0)\exp(-i\delta'(iu_0))$ and $u_0=\ln W$. Hence

$$\gamma_2-\gamma_1\sim(-4\exp^{-i\delta'(iu_0)}\sinh u_0^2 e^{u_0}/\sinh\gamma_0)e^{-Mu_0}. \tag{4.12}$$

This means that below $T_{w,M}(h_1)$ the two highest eigenvalues $\lambda_1=\Lambda_0 e^{-\gamma_1}$ and $\lambda_2=\Lambda_0 e^{-\gamma_2}$ are asymptotically degenerate as $M\to\infty$ and the correlation length $\xi_\parallel$ diverges exponentially with the width of the strip, $\xi_\parallel\sim e^{+Mu_0}$.[16]

In the scaling limit $u_0\to 0$, $n\equiv M-1\to\infty$ but $X\equiv nu_0=O(1)$ γ_1 is given by (4.6) and

$$\gamma_2-v_0=-(1/4\sinh v_0)u_0^2(1+2e^{-X})^2+O(u_0^3), \tag{4.13}$$

from which the scaling for the correlation length follows

$$\xi_\parallel=n^2(\sinh v_0/2)X^{-2}e^X. \tag{4.14}$$

At $T_{w,M}(h_1)$ γ_2 becomes equal to v_0 and above $T_{w,M}(h_1)$ ω_2 switches from imaginary value to the real root of (3.33) between 0 and π/M. At the same time ω_1 remains imaginary up to the $T_w(h_1)$ when in turn γ_1 becomes equal v_0 and ω_1 switches to the real value. Between $T_{w,M}(h_1)$ and $T_w(h_1)$ there is a crossover from the nonwet to the wet regime. In a wet regime both ω_1 and ω_2 are real roots of (3.33) with $0<\omega_1<\pi/M$ and $\pi/M<\omega_2<2\pi/M$. For large M and at the temperature fixed at any value below $T_{c,\infty}$, ω_1 is given by (4.8) and $\omega_2=2\pi M^{-1}+(A_1+B_1)\pi M^{-2}+\cdots$. Expanding (3.8) in powers of $1/M$ we find

$$1/\xi_\parallel=\gamma_2-\gamma_1=(3/2\sinh v_0)\pi^2 M^{-2}. \tag{4.15}$$

The above result shows that the finite-size dependence of $\xi_\parallel$ above $T_w(h_1)$ with weakening of bonds is the same as for the planar fluctuating interface in the capillary-wave dominant regime, found for large $(+/-)$ Ising strips with no weakening of bonds $(a_1=a_2=1)$.[16,20,22]

The result (4.15) is a particular case of a more general scaling law[22] of the form

$$M/\xi_\parallel=Y(M\sinh v_0),$$

and the leading term of the low-temperature (large argument) expansion of the scaling function Y produces (4.15).[22] Small argument expansion recovers finite-size scaling near $T_{c,\infty}$.[22] This can be understood by combining (4.10) and (3.8).

B. The case of $h_1h_2<0$ and $|h_1|\neq|h_2|$

The qualitative behavior of the surface tension below the highest of the wetting temperatures, which we take to be $T_w(h_1)$, is the same as for the previous case, although the expression for γ_1 is more complicated. For fixed temperature below $T_w(h_1)$ and for large M it takes the form

$$\gamma_1=\gamma_{01}-C'(T,h_1,h_2)\exp(-Mu_{01}) \tag{4.16}$$

with the constant

$$C'(T,h_1,h_2)=\frac{2(e^{u_{01}}\sinh^2 u_{01}(1-W_2W_1)}{\sinh\gamma_{01}(W_2W_1^{-1}-1)}\times\exp(-2i\delta'(iu_{01})). \tag{4.17}$$

Here

$$\cosh\gamma_{01}=\cosh v_0+1-\cosh u_{01} \tag{4.18}$$

and $u_{01}\equiv\ln W_1$. Hence, below $T_w(h_1)$ the surface tension is exponentially close to the value γ_{01}/β which is the surface tension of the bound interface in the semi-infinite Ising system with a single h_1 wall.

Derivation of the scaling form for the singular part of the surface tension in the vicinity of $T_w(h_1)$ is similar to that for the case of the perfect asymmetry. We take the scaling variable to be $X\equiv u_{01}n$ and in the limit $n\to\infty$, $u_{01}\to 0$ but $X=O(1)$ we find

$$\gamma_1-v_0=n^{-2}F_1(X) \tag{4.19}$$

with the scaling function $F_1(X)=(1/2\sinh v_0)X^2(1-2e^{-2X})^2$.

For the case of $h_1h_2<0$ and $|h_1|\neq|h_2|$ there is no asymptotic degeneracy of the two highest eigenvalues. For fixed temperature below $T_w(h_1)$ and $T_w(h_2)$, when both ω_1 and ω_2 are purely imaginary, γ_1 lies exponentially close to the value γ_{01} given by (4.18) and γ_2 lies exponentially close to the value γ_{02} given by

$$\cosh\gamma_{02}=\cosh v_0+1-\cosh u_{02}. \tag{4.20}$$

Hence

$$1/\xi_\parallel=\gamma_2-\gamma_1\sim\gamma_{02}-\gamma_{01} \tag{4.21}$$

up to the exponentially small corrections. When the perfect asymetry $h_1=-h_2$ is broken, the correlation length $\xi_\parallel$, instead of diverging with M exponentially, is an M *independent* function of temperature only. This result was not suggested earlier.

Between $T_w(h_2)$ and $T_w(h_1)$ or more precisely between $T_{w,M}(h_2)$ and $T_{w,M}(h_1)$, the value of ω_1 remains purely imaginary but ω_2 switches to the real value. The finite-size dependence becomes more evident in this crossover region. If $T_w(h_2)$ lies sufficiently far from $T_w(h_1)$ the asymptotics for large M and fixed temperature of γ_1 and γ_2 is different. γ_2 is given by

$$\gamma_2=v_0+(1/2\beta\Gamma)\pi^2M^{-2}+O(M^{-3}), \tag{4.22}$$

and as far as the temperature is not too close to the $T_w(h_1)$, the asymptotic behavior of γ_1 is still given by (4.11). Above $T_w(h_1)$ the behavior of the surface tension $\sigma(M)$ and longitudinal correlation length is up to the highest order of $1/M$ the same as for the case of the perfect asymmetry system.

Our results for $\xi_\parallel$ are summarized in Figs. 1–3. Figure 1 shows the test of scaling (4.14) in the nonwet regime. Figure 2 shows the comparison of three strips of the same width: a $(+/+)$ strip, a $(+/-)$ strip with perfect asymmetry, and the $(+/-)$ strip with broken asymmetry (broken by a slight difference between the two surface fields, $a_2=a_1+\epsilon$). First,

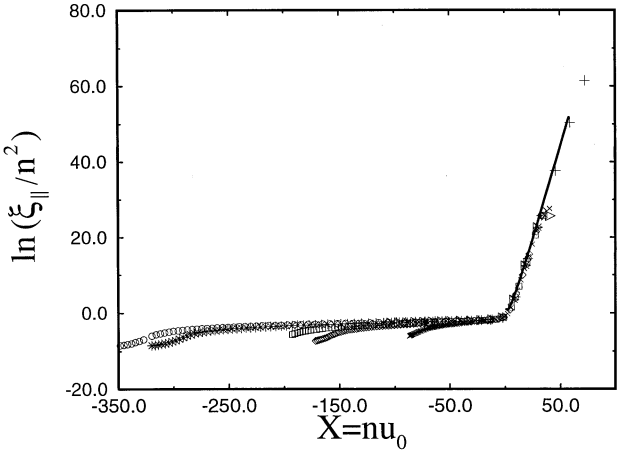

FIG. 1. Scaling for the correlation length $\xi_{\|}$ in a direction parallel to the walls. $\ln(\xi_{\|}/n^2)$ is plotted as function of $y=nu_0$ for $a_1=a_2=0.9$ and different strip widths $n=M-1$: (a) circles for $n=200$, (b) stars for $n=180$, (c) squares for $n=120$, (d) diamonds for $n=96$, and (e) plus for $n=48$. $T_w(M\to\infty)\sim 0.488\,04\ T_{c,\infty}$. The solid curve represents the scaling function given by (4.14).

above $T_{c,\infty}$, $\xi_{\|}(T)$ is common to all strips. On lowering the temperature, at $T_{c,\infty}$ the $(+/-)$ strips show smooth further increase. Hence only the $(+/+)$ strip shows a peak at $T_{c,\infty}$. Between $T_{c,\infty}$ and T_w [and beyond $T_w(M)$], $\xi_{\|}(T,M)$ is practically *independent* of ϵ. Below $T_w(M)$, $\xi_{\|}$ of the perfectly antisymmetric system ($\epsilon=0$) continues to rise,

$$\xi_{\|}\sim P(W)W^M$$

with the prefactor $P(W)$ which follows from Eq. (4.12); temperature dependence of W is given by (3.27) and W increases

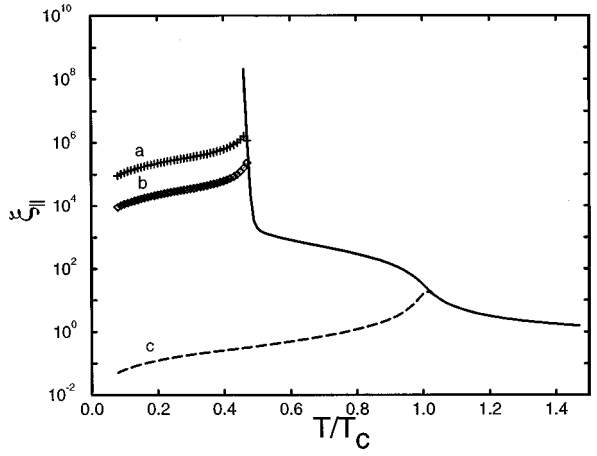

FIG. 2. Comparison of three strips:$(+/+)$, $(+/-)$ with perfect asymetry $(a_1=a_2)$,$(+/-)$ with symmetry broken by unequal surface fields, $a_2=a_1+\epsilon$: $M=97$, $a_1=0.9$. Full line: $(+/-)$ strips for $\epsilon=0$. Dashed line labeled (c): $(+/+)$ strip; indistinguishable from the full line above $T_{c,\infty}$. Curves marked (a) and (b) ($\epsilon=10^{-7},10^{-5}$, respectively) calculated from (4.21), (4.20), (4.18), (3.27), and (3.30) assuming $v_4=v_3+2K_2\epsilon$. The points show numerically exact computation, crosses for $\epsilon=10^{-7}$, diamonds for $\epsilon=10^{-5}$. These points join the full line as shown and continue at all higher temperatures indistinguishable from the full line. Note the logarithmic scale. See Fig. 3.

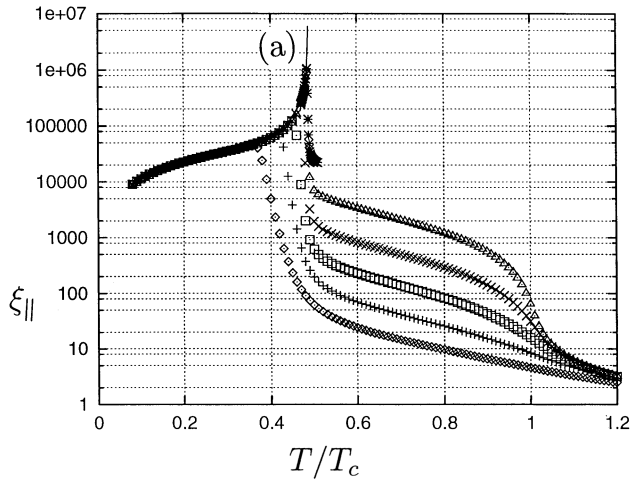

FIG. 3. Plot of $\xi_{\|}(T,M,\epsilon)$ for $\epsilon=0.000\,01$, $M=12$ (diamonds), 24 (crosses), 48 (squares), 96 (crosses), 200 (triangles), and 400 (stars). Each M value has a different crossover point (in fact a small region) where $\xi_{\|}(T)$ joins the common low-temperature line independent of M, marked (a) and calculated with approximations described in Fig. 2 and in the text.

indefinitely as T decreases. This was predicted.[16] In contrast to that, any system with broken symmetry by $\epsilon\neq 0$ crosses over (very abruptly for large M) to a curve $\xi_{\|}(T,\epsilon)$ *common* to all M. Two such curves (for $\epsilon=10^{-5}$ and 10^{-7}) are shown in Fig. 2. These were calculated from (4.21) with (4.20), (4.18), (3.27), and (3.30) assuming $v_4=v_3+2K_2\epsilon$. These equations describe a superposition of two semiinfinite wall-spin systems without any interference. These $d=2$ plots differ from Fig. 13 of Ref. 16 which refers to $d=3$ systems. Another remark concerns the prediction of Eq. (4.15): the region where this scaling law operates is rather limited. Its derivation from the more general scaling law[22] requires that $T\ll T_{c,\infty}$ and, on the other hand we must have $T\gg T_w$, especially for small M (see Fig. 3).

Figure 3 shows a plot similar to Fig. 2, of data computed without approximations for one value of ϵ and several values of M of the $(+/-)$ strip. The low-temperature branch is indeed common to all values of M (for $M>10$, say).

From the eigenvalues one can also compute the free energy per column and by numerical differentiation we have computed the heat capacities. Figure 4(a) shows a family of curves with different M for perfect asymmetry. The strong peak near $T/T_c=1$ follows the usual finite-size scaling and nothing new is revealed in relation to the work of Fisher and co-workers (see Ref. 5 where references to earlier work can be found). The peaks of the $(+/-)$ strips are some 20% lower than those for the $(+/+)$ strips. The perfectly antisymmetric system differs only quantitatively from systems with $|h_1|\neq|h_2|$. Near T_w, as $M\to\infty$, the surface peak in C_v (per column) approaches the second-order finite discontinuity found by Abraham[4] in a semi-infinite system with one wall. To extract the singular part, we should form the difference $[\sigma(\text{wall, phase2})\text{-}\sigma(\text{wall, phase1})\text{-}\sigma(\text{phase1, phase2})]\sim -|t|^{2-\alpha}$ which in our case of two perfectly antisymmetric walls translates into $\beta f(\text{strip}(+/-))-\beta f(\text{strip}(+/+))-v_0$. In fact the difference $C_v(+-)-C_v(++)=(d/dT)(d/d\beta)\gamma_1(T,M)$ and γ_1 has the mean-

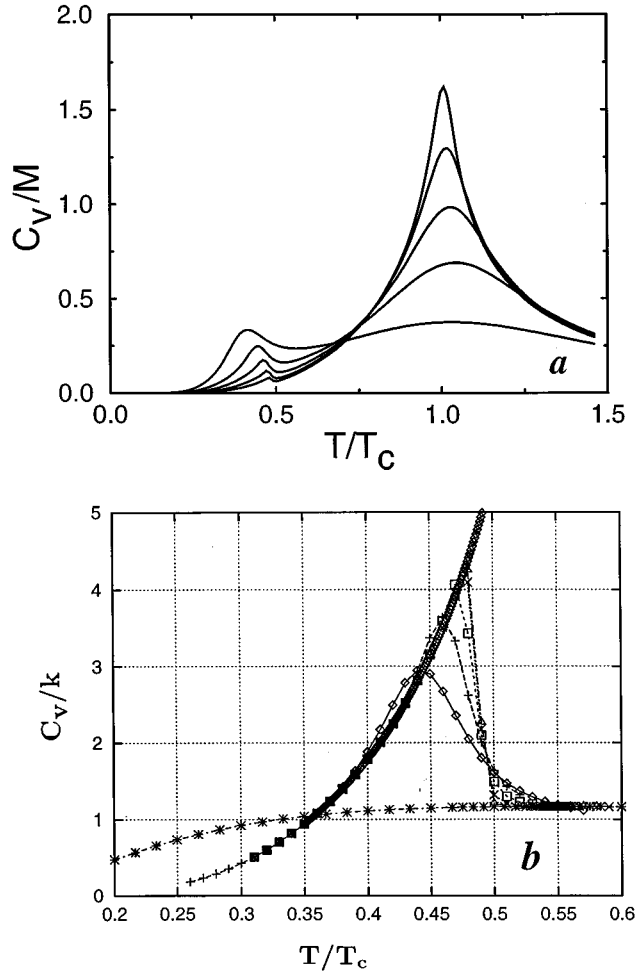

FIG. 4. (a) Heat capacity C_v/k divided by strip width M (heat capacity per site in units of Boltzmann constant k) plotted against temperature $T/T_{c,\infty}$ for $M=12,24,48,96,200$. Increased M raises the peak near $T_{c,\infty}$ but decreases the rounded step near T_w. (b) Heat capacity ''per column'' obtained by remultiplying by M. $M=12,24,48,96,200$ (diamonds, crosses, squares, x crosses, and triangles, respectively); the contribution of v_0 (stars); the contribution of γ_0 (densely spaced diamonds). The rounded step near T_w is sharper and slightly higher for larger M—bounded by $\Delta C_v/k$ which follows from exact equations (Ref. 4) for the semiinfinite system. These predict γ_0 from Eq. (4.4) for $T<T_w$ and v_0 for $T>T_w$.

ing of a surface free energy $/kT$. The plot in Fig. 4(b) shows the surface heat capacity $C_s=C_v(+-)-C_v(++)$. The heat capacity of the Onsager free interface (not yet subtracted) of surface tension $v_0=v_2-v_1$ is also shown (as the flat background curve). The scaling law (4.7) for the singular part of the surface tension requires further subtraction of the v_0 contribution and the singular part of heat capacity of the $(+/-)$ strip thus obtained should scale with $X\equiv nu_0$; this scaling is not satisfactory. Apparently the corrections to scaling are numerically not small. In fact already the scaling of $\beta\sigma$ shown in Fig. 5 is not as excellent as in typical bulk scaling plots as soon as X is not close to zero.

V. MAGNETIZATION PROFILES

Formal expressions for the average magnetization $\langle\sigma_m\rangle$ depend on the relative signs of the surface fields. The

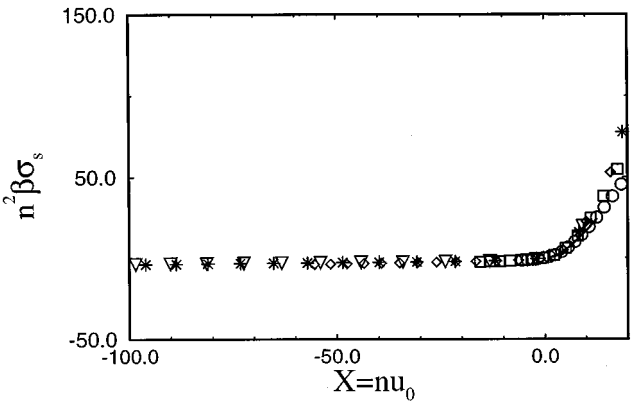

FIG. 5. Scaling for the surface excess free energy (per unit area) σ_s given by (4.2). $n^2\beta\sigma_s$ is plotted as function of $y=nu_0$ for fixed $a_1=a_2=0.9$ and different n: (a) stars for $n+1=201$, (b) triangles down for $n+1=181$, (c) diamonds for $n+1=97$, (d) squares for $n+1=49$, (e) circles for $n+1=25$. Wetting temperature for $h_1=0.9$ K is $T_w(h_1)\sim 0.488\ T_{c,\infty}$. The solid curve represents the scaling function $F(x)$ given by (4.7).

transfer-matrix spectrum obtained in the previous sections includes all four choices of these signs. To extract the suitable case we used the projection operators.

The formula for an average of any operator A has the form

$$\langle A\rangle=\mathrm{Tr}(V^N P_1 A P_2)/\mathrm{Tr}(V^N P_1 P_2), \tag{5.1}$$

where P_1 and P_2 are the projection operators and we wish to take the limit of the infinite long strip $N\to\infty$.

For the case of the surface fields of the opposite signs, say $(-/+)$, i.e., $h_1<0$, $h_2>0$, the projection operators used in (6.1) are given by (2.12) for P_1 and (2.13) for P_2. In the limit of large N the largest eigenvalues dominate and in the representation in which V is diagonal we obtain

$$\begin{aligned}\lim_{N\to\infty}\mathrm{Tr}(V^N P_1 A P_2)=(1/2)\Lambda_1^N[&\langle 0|f_1 A f_1^\dagger|0\rangle\\ &+\langle 0|f_1 f_0 A f_0^\dagger f_1^\dagger|0\rangle-\langle 0|f_1 A f_0^\dagger f_1^\dagger|0\rangle\\ &-\langle 0|f_1 f_0 A f_1^\dagger|0\rangle].\end{aligned} \tag{5.2}$$

The largest eigenvalue Λ_1 is equal to $\Lambda_1=\Lambda_0\exp(-\gamma_1)$ and Λ_0 is given by (2.11). The average magnetization $\langle\sigma_m\rangle$ where m is the height index $m=1,2,\ldots,M-1$ is the average of the operator σ_m^x, counting spins at the position m. This operator is nonlocal in the spinor representation

$$\sigma_m^x=\Gamma_0\Gamma_1\cdots\Gamma_{2m}. \tag{5.3}$$

Substituting σ_m^x for A and commuting $f_0\Gamma_0$ we obtain

$$\langle\sigma_m\rangle=-(i)^m\langle 0|f_1\Gamma_0\Gamma_1\cdots\Gamma_{2m}f_1^\dagger|0\rangle, \tag{5.4}$$

already in the limit $N\to\infty$. If both walls prefer the same, say $(+)$ phase, i.e., $h_1,h_2>0$, the projection operators for the $(+/+)$ system are $P_1=(1/2(f_0+f_0^\dagger-I)$ and $P_2=(1/2)[(f_0-f_0^\dagger)P+I]$ [see (2.15) and (2.16)]; now the largest eigenvalue which contributes is $\Lambda_1=\Lambda_0$ and after the similar algebra one has

$$\langle\sigma_m\rangle=-(i)^m\langle 0|\Gamma_0\Gamma_1\cdots\Gamma_{2m}|0\rangle, \tag{5.5}$$

in the limit $N\to\infty$. The exact formulas (5.4), (5.5) for $\langle\sigma_m\rangle$ can be transformed into a form suitable for practical computations by using Wicks theorem and by simplifying the Pfaffian expression for $\langle\sigma_m\rangle$ to a determinant of a certain matrix B (in a way similar to that described in Ref 12.) The main steps of this computation are the following. The Wicks theorem transforms the average of an ordered product of anticommuting operators into a Pfaffian of an antisymmetric matrix A

$$\langle\sigma_m\rangle=-(i)^m\mathrm{Pf}A=-(i)^m\det(A)^{1/2}. \tag{5.6}$$

We discuss the case of opposite surface fields $(-/+)$ first. For this case the matrix A has a dimension $(2m+2)\times(2m+2)$ with the elements which are averages of products of only two operators (so-called contractions)

$$A_{0j}=\langle 0|f_1\Gamma_j|0\rangle \quad (j=1,\ldots,2m), \tag{5.7}$$

$$A_{0,2m+1}=\langle 0|f_1 f_1^{\dagger}|0\rangle=1, \tag{5.8}$$

$$A_{i,2m+1}=\langle 0|\Gamma_i f_1^{\dagger}|0\rangle \quad (i=1,\ldots,2m), \tag{5.9}$$

$$A_{i,j}=\langle 0|\Gamma_i\Gamma_j|0\rangle \quad (i=2,\ldots,2m, \quad j=3,\ldots,2m+1), \tag{5.10}$$

$$A_{ii}=0, \quad A_{ij}=-A_{ji} \quad (i,j=0,\ldots,2m+1). \tag{5.11}$$

We can express contractions in terms of the elements of the orthogonal matrix S defined in Sec. II [Eq. (2.23)] and calculated in Sec. III. S is the matrix of linear transformation of spinors Γ_i into spinors g_k (see Sec. II)

$$\Gamma_i=\sum_m S_{i,m}g_m \quad (i,m=0,\ldots,2M+1). \tag{5.12}$$

The elements of matrix S are built up from the real $\xi(\omega_k)$ and imaginary $\eta(\omega_k)$ parts of eigenvectors y given by (3.18) according to Eq. (2.23) and are functions of the wave number ω_k. They can be oscillatory or exponential functions of ω—depending on whether ω_k is real or imaginary—however, the structure of the matrix S is always the same.

The 0th row and column and $2M+1$ row and column have vanishing elements except for $S_{00}=S_{2M+1,2M+1}=1$ hence it is enough to consider a $2M\times 2M$ matrix S. The columns are ordered according to $k=1,\ldots,M$, i.e., the $2k$ and $2k-1$ columns belong to $k,\omega=\omega_k$. Then

$$S_{2n-1,2k-1}=\eta_{2n-1}, \quad n=1,\ldots,M, \tag{5.13}$$

$$S_{2n-1,2k}=0, \quad n=1,\ldots,M, \tag{5.14}$$

$$S_{2n,2k}=\xi_{2n}, \quad n=1,\ldots,M, \tag{5.15}$$

$$S_{2n,2k-1}=0, \quad n=1,\ldots,M. \tag{5.16}$$

For ω_k real we found an oscillatory behavior of $\eta(\omega_k)$ and $\xi(\omega_k)$:

$$\eta_1(\omega_k)=-\mathcal{A}(v_3)C\left[\sinh\frac{v_2}{2}\cos\frac{1}{2}[-\omega_k+\delta^*(\omega_k)-\psi(\omega_k)]+\cosh\frac{v_2}{2}\cos\frac{1}{2}[\omega_k+\delta^*(\omega_k)+\psi(\omega_k)]\right], \tag{5.17}$$

$$\eta_{2n+1}(\omega_k)=C\cos\frac{1}{2}[(2n-1)\omega_k+\delta^*(\omega_k)-\psi(\omega_k)], \quad (n=1,\ldots,M-2), \tag{5.18}$$

$$\eta_{2M-1}(\omega_k)=\mathcal{A}(v_4)C\left[\sinh\frac{v_2}{2}\cos\frac{1}{2}[(2M-3)\omega_k-\delta^*(\omega_k)-\psi(\omega_k)]+\cosh\frac{v_2}{2}\cos\frac{1}{2}[(2M-3)\omega_k+\delta^*(\omega_k)-\psi(\omega_k)]\right], \tag{5.19}$$

$$\eta_{2n}(\omega_k)=0 \quad (n=1,\ldots,M), \tag{5.20}$$

and

$$\xi_2(\omega_k)=\mathcal{B}(v_3)C\left[\sinh\frac{v_2}{2}\cos\frac{1}{2}[-\omega_k+\delta^*(\omega_k)-\psi(\omega_k)]+\cosh\frac{v_2}{2}\cos\frac{1}{2}[\omega_k+\delta^*(\omega_k)+\psi(\omega_k)]\right], \tag{5.21}$$

$$\xi_{2n+2}(\omega_k)=C\cos\frac{1}{2}[(2n-1)\omega_k-\delta^*(\omega_k)-\psi(\omega_k)], \quad (n=1,\ldots,M-2), \tag{5.22}$$

$$\xi_{2M}(\omega_k)=-\mathcal{B}(v_4)C\left[\sinh\frac{v_2}{2}\cos\frac{1}{2}[(2M-3)\omega_k-\delta^*(\omega_k)-\psi(\omega_k)]+\cosh\frac{v_2}{2}\cos\frac{1}{2}[(2M-3)\omega_k+\delta^*(\omega_k)-\psi(\omega_k)]\right], \tag{5.23}$$

$$\xi_{2n-1}(\omega_k)=0 \quad (n=1,\ldots,M). \tag{5.24}$$

Here $C=2\sqrt{2B_1}$ and B_1 [see (3.18)] is determined from the normalization condition for the eigenvector $y(\omega_k)$ (2.22). The constants $\mathcal{A}(v_i)$ and $\mathcal{B}(v_i)$, $i=3,4$ are given by (3.19a) and (3.19b), respectively. The function $\psi(\omega_k)$ is defined as [see (3.20)]

$$e^{i\psi}\equiv R(e^{i\omega})=-i\,\frac{T_1+ie^{-\gamma}qz\sinh v_1}{T_1qz-ie^{-\gamma}\sinh v_1}.$$

For ω imaginary $\omega=iv$ the components of the eigenvector $y(\omega)$ are exponential functions of v

$$\eta_1(v)=-\mathcal{A}(v_3)C_1\left[\sinh\frac{v_2}{2}\,[e^{i\delta^*(iv)}e^{-v}+R(v)e^{-2v}]+\cosh\frac{v_2}{2}\,[e^{-v}+R(v)e^{i\delta^*(iv)}e^{-2v}]\right], \tag{5.25}$$

$$\eta_{2n+1}(v)=C_1[e^{i\delta^*(iv)}e^{-(n+1)v}+R(v)e^{(n-2)v}], \tag{5.26}$$

$$\eta_{2M-1}(v)=\mathcal{A}(v_4)C_1\left[\cosh\frac{v_2}{2}\,[e^{i\delta^*(iv)}e^{-Mv}+R(v)e^{(M-3)v}]+\sinh\frac{v_2}{2}\,[e^{-vM}+R(v)e^{i\delta^*(iv)}e^{(M-3)v}]\right], \tag{5.27}$$

$$\eta_{2n}(v)=0\quad(n=1,\ldots,M), \tag{5.28}$$

and

$$\xi_2(v)=\mathcal{B}(v_3)C_1\left[\sinh\frac{v_2}{2}\,[e^{i\delta^*(iv)}e^{-v}+R(v)e^{-2v}]+\cosh\frac{v_2}{2}\,[e^{-v}+R(v)e^{i\delta^*(iv)}e^{-2v}]\right], \tag{5.29}$$

$$\xi_{2n+2}(v)=C_1[e^{-(n+1)v}+R(v)e^{i\delta^*(iv)}e^{(n-2)v}], \tag{5.30}$$

$$\xi_{2M}(v)=-\mathcal{B}(v_4)C_1\left[\cosh\frac{v_2}{2}\,[e^{i\delta^*(iv)}e^{-Mv}+R(v)e^{(M-3)v}]+\sinh\frac{v_2}{2}\,[e^{-vM}+R(v)e^{i\delta^*(iv)}e^{(M-3)v}]\right], \tag{5.31}$$

$$\xi_{2n-1}(v)=0\quad(n=1,\ldots,M). \tag{5.32}$$

Here $C_1=\sqrt{2}B_1$ and $R(v)$ is given by (3.26) for $z^2=e^{i\omega}=e^{-v}$.

In terms of the elements of matrix S the contractions read

$$\langle 0|\Gamma_i\Gamma_j|0\rangle=0,\quad i,j=\text{both odd or both even}, \tag{5.33}$$

$$\langle 0|\Gamma_i\Gamma_j|0\rangle=i\sum_{k=1}^{M}S_{i,2k}S_{j,2k-1}-S_{i,2k-1}S_{j,2k}\quad(i<j), \tag{5.34}$$

$$\langle 0|f_1\Gamma_j|0\rangle=S_{r,2}+iS_{r,1}, \tag{5.35}$$

$$\langle 0|\Gamma_i f_1^{\dagger}|0\rangle=S_{r,2}-iS_{r,1}. \tag{5.36}$$

However, $S_{r,2}=0$ for r odd and $S_{r,1}=0$ for r even so the antisymmetric matrix A takes the following form:

$$A=\begin{pmatrix}0 & iS_{11} & S_{22} & \cdots & 1\\ \cdots & 0 & Q_{12} & \cdots & -iS_{11}\\ \vdots & \vdots & 0 & \mathbf{Q} & \vdots\\ \cdots & \cdots & \cdots & \cdots & \cdots\\ \cdots & \cdots & \cdots & \cdots & 0\end{pmatrix},$$

where we abbreviate

$$Q_{ij}=0\quad i,j=\text{both odd or both even, otherwise,}$$

$$Q_{ij}=\sum_{k=1}^{M}S_{i,2k}S_{j,2k-1}-S_{i,2k-1}S_{j,2k}\quad(i<j). \tag{5.37}$$

After some manipulations on this matrix in order to group zeros together (Ref. 12) we obtain the very useful result that $\det(A)=[\det(B)]^2$ so

$$\langle\sigma_m\rangle=-\det(B) \tag{5.38}$$

with

$$B=\begin{pmatrix}1 & 2S_{11} & 2S_{31} & 2S_{51} & \cdots\\ S_{22} & -iQ_{21} & -iQ_{23} & -iQ_{25} & \cdots\\ S_{42} & -iQ_{41} & -iQ_{43} & -iQ_{45} & \cdots\\ \vdots & \vdots & \vdots & \vdots & \end{pmatrix}.$$

The elements of matrix B are the same for all $m=1,\ldots,M-1$; the dimension of B is $(m+1)\times(m+1)$.

For the system with the surface fields of the *same* sign, say $(+/+)$, the matrix B has a dimension $m\times m$ and can be obtained from the matrix B of the $(-/+)$ system by deleting the first column and first row.

Equations (3.39) have been implemented for numerical computation of the magnetization profiles $\langle\sigma_m\rangle$ in the case of the opposite surface fields. We used $M\in[9,201]$ and $a_1,a_2\in(0,1)$.

For the perfect asymmetry system $h_1=-h_2$ a selection of the magnetization profiles computed for a fixed width of the strip $n\equiv M-1$, a fixed value of the parameter $a_1=a_2$ and at different temperatures is shown in Figs. 6, 7, and 8. As can be expected from the symmetry features of the system all the profiles are antisymmetric

$$\langle\sigma_m\rangle=-\langle\sigma_{M-m}\rangle \tag{5.39}$$

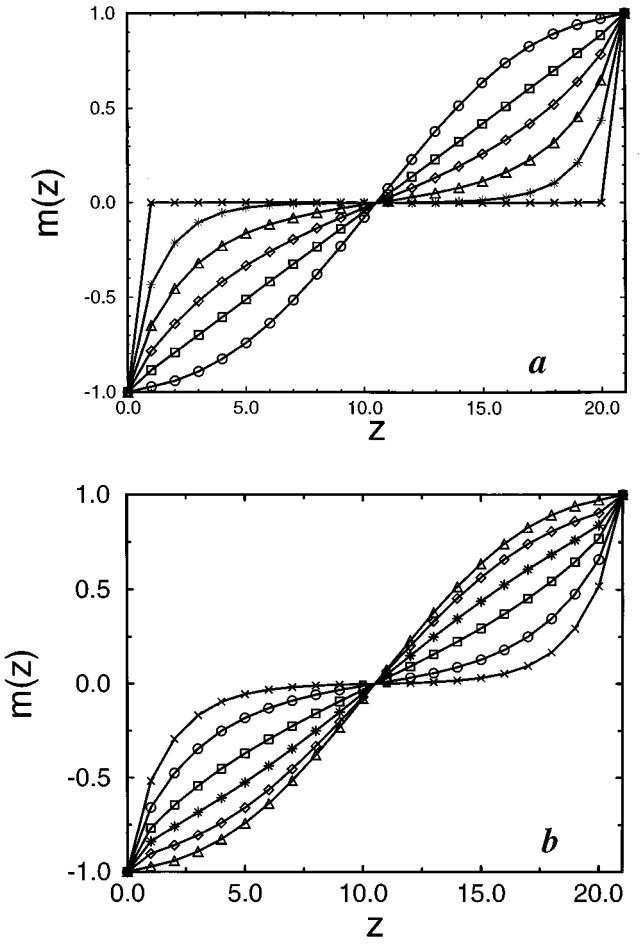

FIG. 6. A selection of computed magnetization profiles for fixed $n=20$ and perfect asymmetry with $a_1=a_2=0.9$, showing the variation with temperature (in units of $T_{c,\infty}$); (a) crosses, $T/T_{c,\infty}=0.3$; stars, $T/T_{c,\infty}=0.45$; triangles up for $T/T_{c,\infty}=0.465$; diamonds for $T/T_{c,\infty}=0.475$; squares for $T\sim T_w(M\to\infty)$; circles for $T/T_{c,\infty}=0.5$. (b) triangle up for $T/T_{c,\infty}=0.6$; diamonds for $T/T_{c,\infty}=0.8$; stars for $T\sim T_{c,\infty}$; squares for $T/T_{c,\infty}=1.05$; circles for $T/T_{c,\infty}=1.1$; crosses for $T/T_{c,\infty}=1.4$. The wetting temperature $T_w(M\to\infty)\sim 0.488\,04\ T_{c,\infty}$. Curves are drawn only as guides for the eye.

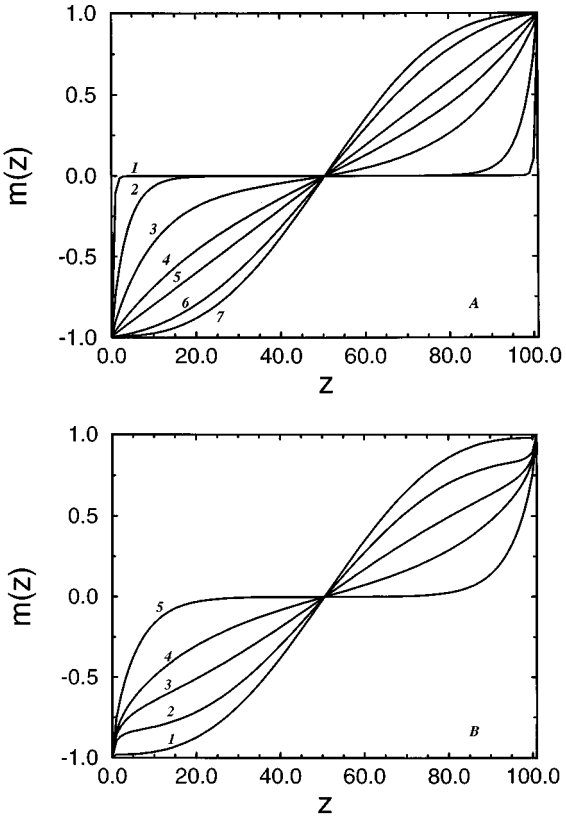

FIG. 7. A selection of magnetization profiles computed for larger system $n=100$ with the perfect asymmetry and the same surface fields ($a_1=a_2=0.9$), for various temperatures in units of $T_{c,\infty}$: (a) (1) for $T/T_{c,\infty}=0.3$; (2) for $T/T_{c,\infty}=0.45$; (3) for $T/T_{c,\infty}=0.482$; (4) for $T/T_{c,\infty}=0.488$; (5) for $T\sim T_w(h_1)$; (6) for $T/T_{c,\infty}=0.5$, and (7) for $T/T_{c,\infty}=0.6$. (b) (1) for $T/T_{c,\infty}=0.9$; (2) for $T/T_{c,\infty}=0.99$; (3) for $T\sim T_{c,\infty}$; (4) for $T/T_{c,\infty}=1.025$; (5) for $T/T_{c,\infty}=1.1$. The wetting temperature $T_w(h_1)\sim 0.488\,04\ T_{c,\infty}$. The lines are drawn through all 101 points.

Figures 6(a) and 6(b) show profiles calculated for a relatively narrow strip $n=20$ and large parameter $a_1=a_2=0.9$ which corresponds to *slightly* weakened bonds between the walls and the system. The wetting temperature in this case lies far away from the bulk critical temperature $T_{c,\infty}: T_w(h_1=\sigma_0 a_1 J)/T_{c,\infty}\sim 0.488\,04$. For low enough temperatures [crosses in Fig. 6(a)] the average magnetization at all points across the strip is almost zero. As the temperature is increased, the profile gradually changes its shape with the most rapid change taking place near the wetting temperature $T_w(h_1)$. The typical profile in this temperature region is monotonic with the inflection point in the middle of the strip. It quickly increases or decreases in the vicinity of the walls and is concave in the first half of the strip. At $T_w(h_1)$ the profile becomes linear across the whole strip. Above $T_w(h_1)$ it starts to bend, forming eventually a characteristic for the single soft-mode phase interfacelike profile. This profile is convex in the first half of a strip with plateaus of pseudobulk phases near the walls.

The soft-mode profile calculated for $T/T_{c,\infty}=0.6$ and $n=20$ is shown in Fig. 6(a) (circles). For such a small system ($n=20$) all the points of the system ''feel'' the presence of both walls, hence there are almost no plateaus of pseudobulk phases near the walls. These are better seen in Fig. 7(a) (curve 7) calculated for a large system $n=100$.

With the further increase of the temperature, the interfacelike profile starts to deform towards the critical profile at $T_{c,\infty}$ [curve with stars in Fig. 6(b)] and then above $T_{c,\infty}$ it bends once again to be concave in the first half of the strip. Then the system reaches the high-temperature situation in which $\langle\sigma_m\rangle=0$ for all m except for a few sites at the walls.

The convexity of the profile can be connected with the type of eigenvectors y_k, $k=1,\ldots,2M$ as functions of the ''wave number'' ω. As we know from Sec. III, below the wetting temperature $T_w(h_1)$ both ω_1 and ω_2 are imaginary $\omega_1=iv_1$, $\omega_2=iv_2$. This implies that the first four columns of the orthogonal matrix S [these are real and imaginary parts of the eigenvectors $y_1(\omega_1)$ and $y_2(\omega_2)$ see Eq. (2.23)], consist of exponential functions of v_1 and v_2. This in turn results in the shape of the profiles which are concave in the first half of the strip. Also above $T_{c,\infty}$ there is the same convexivity of the profile although this time there is only one imaginary wave number $\omega_1=iv$ and hence only two columns of the

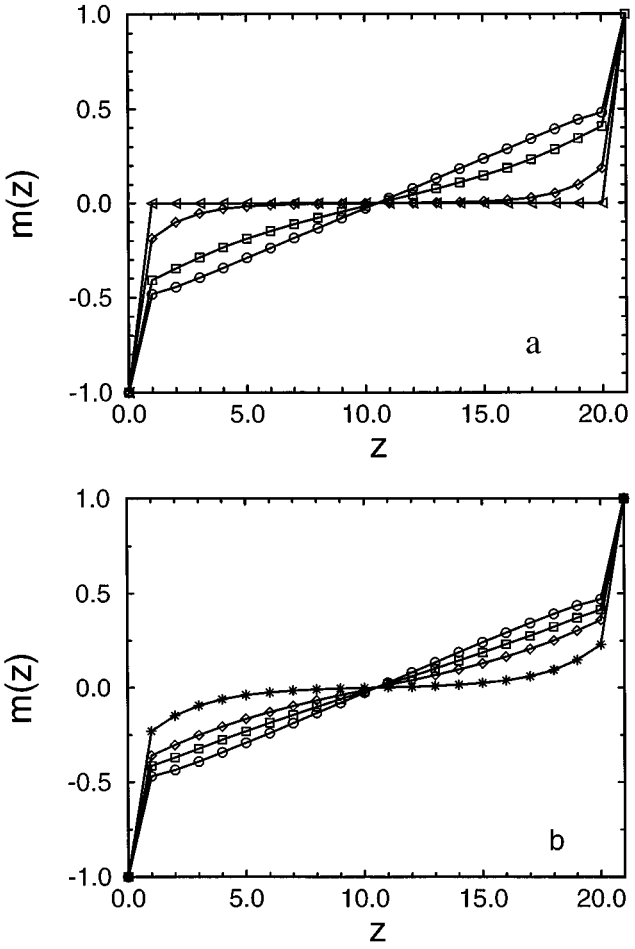

FIG. 8. A selection of magnetization profiles computed for small system $n=20$ with the perfect asymmetry and weaker surface fields $-a_1=a_2=0.3$ for various temperatures in units of $T_{c,\infty}$: (a) triangle left for $T/T_{c,\infty}=0.3$; diamonds for $T/T_{c,\infty}=0.7$; squares for $T/T_{c,\infty}=0.9$; circles for $T\sim T_w(h_1)$. (b) circle for $T/T_{c,\infty}=0.985$; squares for $T/T_{c,\infty}=1.05$; diamonds for $T/T_{c,\infty}=1.1$; stars for $T/T_{c,\infty}=1.35$. The wetting temperature $T_w(M\to\infty)\sim 0.9665\ T_{c,\infty}$. Curves through these profiles are drawn only as guides for the eye.

matrix S consists of the exponential functions. For the soft-mode phase between $T_w(h_1)$ and $T_{c,\infty}$, all the wave numbers are real so that the elements of the matrix S are oscillatory functions of ω_k, $k=1,\ldots,M$. This results in the profiles being convex in the first half of the strip.

For comparison we also show the magnetization profiles computed for $a_1=a_2=0.9$ [the same $(-/+)$ surface fields as in Fig. 6] but for the large system $n=100$ [Figs. 7(a) and 7(b)]. The profiles look qualitatively similar, the main difference being that for the large system the rapid change in the shape of the profile near $T_w(h_1)$ takes place in a very narrow temperature region about $T_w(h_1)$ and that for wide strips there are well developed plateaus of the ''bulk phases'' near the walls for the soft-mode phase profile.

For completeness we also show the profiles for $n=20$ but for a small parameter $a_1=a_2=0.3$ which corresponds to a large weakening of the bonds between the walls and the system. The wetting temperature in this case lies very close to the bulk critical temperature $T_w(h_1)/T_{c,\infty}\sim 0.95$. Hence there is almost no soft-mode phase with its typical interfacelike profile (Fig. 8).

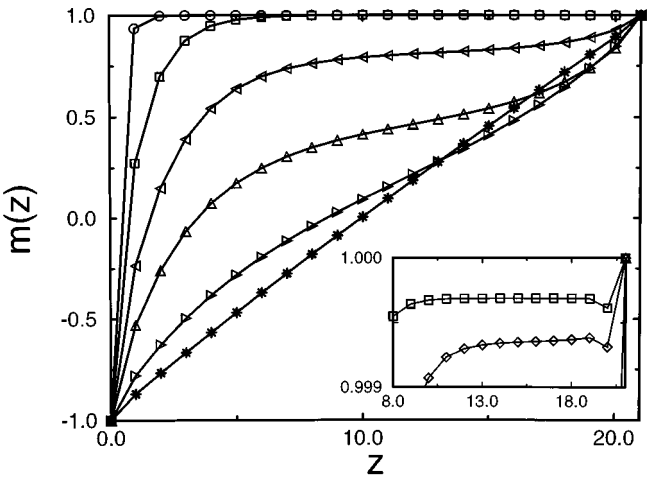

FIG. 9. Magnetization profiles calculated for fixed width of the strip $n=20$ and for surface fields which differ by (a large) $\epsilon=0.001$, $a_1=0.9$ and $a_2=0.899$, for various temperatures below the wetting temperature $T_w(M\to\infty)\sim 0.488\,04\,T_{c,\infty}$: circles for $T/T_{c,\infty}=0.3$; squares for $T/T_{c,\infty}=0.4$; triangles left for $T/T_{c,\infty}=0.45$; triangles up for $T/T_{c,\infty}=0.465$; triangles right for $T/T_{c,\infty}=0.475$; stars for $T\sim T_w$. The profiles are nonmonotonic near the $(+)$ wall as can be seen from the inset with portions of those calculated for $T/T_{c,\infty}=0.4$ (squares) and for $T/T_{c,\infty}=0.42$ (diamonds).

As we have mentioned above, in the region of low temperatures the average magnetization is almost zero for all the points across the strip. This corresponds to the pseudocoexistence of two ''phases'' below the wetting temperature $T_w(h_1)$. One of the profiles of these phases corresponds to a thin film of down spins $(-)$ at wall 1 and a film of up spins $(+)$ at the wall 2 and can be obtained if one breaks the symmetry of the system by applying an infinitesimal bulk field $h\pm 0$ or by setting $a_1=a_2\pm\epsilon$. Figure 9 shows the family of the profiles for one of these phases calculated for the same width of the strip $(n=20)$ as for Fig. 6 and for surface fields which differ by $\epsilon=0.001$, $a_2=0.9$, and $a_1=0.899$. This corresponds to the situation when the spins up $(+)$ phase fills the strip, with a thin film of spins down $(-)$ at wall 1. Also the profiles are nonmonotonic at low temperatures. The average magnetization near the wall that favors the spin-up $(+)$ phase is less than the spontaneous magnetization $+m^*(T)$ of the $(+)$ phase

$$m^*(T)\equiv -[1-(\sinh 2K)^{-4}]^{1/8}. \tag{5.40}$$

This can be seen in the inset of the Fig. 9 although for the small system shown there, only the magnetization in the first two (one) sites at the wall is less than $+m^*(T)$.

With u_0 as a small parameter describing the distance of the system from the wetting temperature we propose and verify the scaling relations for the magnetization profile at the fluctuation-dominated critical wetting transition

$$m(z,T,M)=\mathcal{M}(z/n;nu_0);\quad h=0. \tag{5.41}$$

To check (5.41), we plot $[m(z)-m^*]/m^*$, calculated for different n and different parameter a_1 as a function of z/n for fixed $y=nu_0$ ($\beta_s=1$ for $d=2$ Ising model). Scaling is excellent for a wide range of variable y from $y=20$ up to $y=-10$.

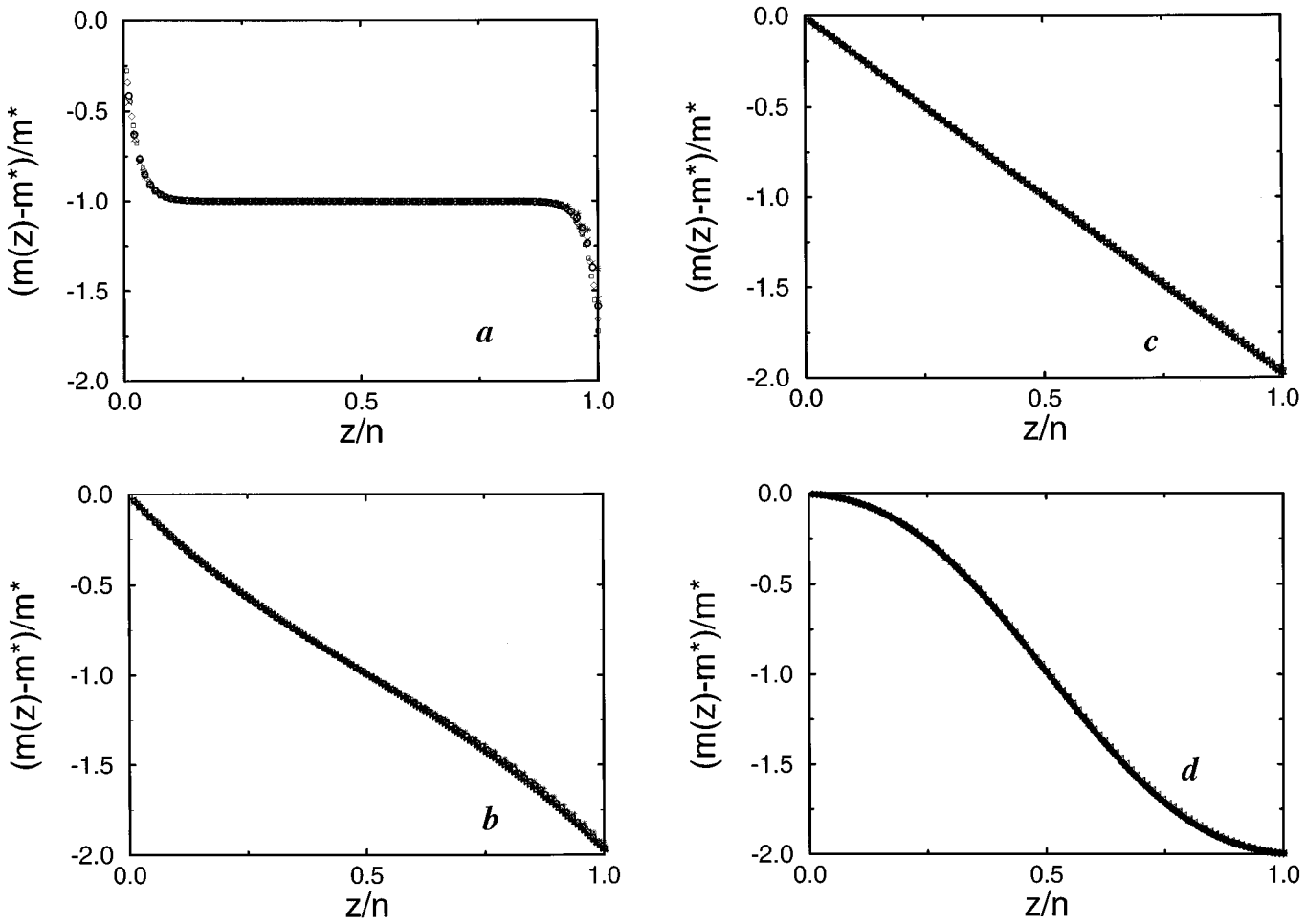

FIG. 10. Scaling of the magnetization profiles for the perfectly asymmetric system, $a_1=a_2$. $[m(z,T,a_1,n)-m^*(T)]/m^*(T)$ is calculated for different widths of the strip n at fixed a_1 and plotted against z/n for the following value of the second scaling variable $y=nu_0$ [see Eq. (5.41)]: (a) $y=20$; (b) $y=1$; (c) $y=0$; (d) $y=-10$. The symbols are circles for the profile calculated for $n=90$ and $a_1=0.9$; squares for $n=150$ and $a_1=0.9$; diamonds for $n=48$ and $a_1=0.9$; crosses for $n=90$ and $a_1=0.8$; stars for $n=120$ and $a_1=0.7$.

Figure 10 shows four scaling functions: (a) for $y=20$ in low-temperature region; (b) for $y=+1$; (c) for $y=0$, i.e., exactly at the wetting temperature $u_0=0$, and (d) for $y=-10$ where the profile is typical for the single soft-mode phase.

For $y=0$ the profile is linear across the whole strip. This linear behavior was found also in the restricted solid-on-solid (RSOS) model[26] with the slope equal to -2. Our profile for $y=0$ is the same as in the RSOS model result. Also our profiles for the soft-mode phase (sufficiently below the bulk critical temperature) perfectly agree with the RSOS result which gives the following prediction:[26]

$$m(z)=m^*[1-2z/n+\pi^{-1}\sin(2\pi z/n)]. \qquad (5.42)$$

The scaling relation for a magnetization profile at the fluctuation-dominated critical wetting transition given by (6.41) is similar to those proposed by Parry, Evans, and Nicolaides[26]

$$m(z,T,M)=\mathcal{M}(zt'^{\beta_s};nt'^{\beta_s}); \quad h=0, \qquad (5.43)$$

where $t'\equiv[T-T_w(h_1)]/T_w(h_1)$. This is because u_0 is proportional to t' near the wetting temperature.

VI. SUMMARY AND CONCLUSIONS

We have presented the transfer-matrix solution for the $d=2$ Ising model confined between parallel walls. The transfer has been taken in such a way as to have the effects of walls incorporated directly into the matrix elements. This solution includes all four possible cases of the sign of the surface fields ($h_1h_2>0$, $h_1h_2<0$). To extract from the general solution the case of the surface fields of equal or opposite signs projection operators have been used. The results are valid for general values of the magnitudes of the surface fields. We have solved the auxiliary eigenvalue problem (2.24) and calculated the exact expressions for the eigenvectors y_k, $k=1,...,2M+1$ [see (3.18)]. In the nonwet regime y_1 and y_2 are exponentially decaying functions of the wave number ω and y_k, $k=3,...,2M+1$ are oscillatory functions of ω. In the wet regime *all* of y_k become oscillatory. These eigenvectors form the orthogonal matrix S which is needed to calculate the magnetization profiles (Sec. V). As the Ising system with the surface fields of equal signs is relatively well understood,[5,14] we concentrate on the case of the surface fields of the opposite signs. In this case the wetting phenomena have proven to be particularly interesting.[16] In an earlier paper[25] we discussed a particular case with only one interac-

tion weakened ($0 \leqslant h_1 \leqslant K\sigma_0, h_2 = -\infty$) and the scaling of magnetization profiles in the near proximity of wall 1. Now we can study any values of h_1, h_2, including the perfectly antisymmetric system with $h_1 = -h_2$. The main features of a system are reflected in the TM spectrum. The highest eigenvalues of $(+/+)$ and $(-/+)$ systems give the singular part of the surface tension $\beta\sigma_s$. The ratio of the two largest eigenvalues for single system gives the correlation length parallel to the walls $\xi_\parallel$ (mass gap). We have studied the asymptotic behavior of $\beta\sigma_s$ and $\xi_\parallel$ in various temperature regions. Within the solution we have distinguished and discussed separately two cases: the perfect asymmetry $h_1 = -h_2$ case and the case $|h_1| \neq |h_2|$, the latter particularly in the context of symmetry breaking by a small difference in (absolute values of) surface fields. We have found that for both cases in the nonwet region the finite-size dependence of the surface tension is weak. The surface tension converges to its bulk value exponentially

$$\sigma(M) - \sigma(\infty) \sim \exp(-M/(u_0^{-1})) \tag{6.1}$$

with characteristic length $u_0^{-1} = 1/\ln W$ for $h_1 = -h_2$ or $u_{01}^{-1} = 1/\ln W_1$ for $|h_1| \neq |h_2|$. u_0^{-1} diverges at the wetting temperature.

In the wet region we find that $\beta\sigma(M)$ converges algebraically to its bulk value [see (4.9)]. The same behavior was obtained for the $(-/+)$ Ising strip with no weakening of bonds $a_1 = a_2 = 1$.[20,21,23]

We have derived analytically the finite-size scaling function for the singular part of the surface tension near $T_w(h_1)$ [Eq. (4.7) for $h_1 = -h_2$ and (4.19) for $|h_1| \neq |h_2|$]. The scaling variable is $X \equiv nu_0$. u_0 is proportional to the variable $t' \equiv [T_w(h_1) - T]/T_w(h_1)$ in the scaling region. This agrees with the earlier proposition of the scaling ansatz[16] near the wetting temperature based on the heuristic arguments. We have also calculated numerically γ_1 and plotted $-n^2\beta\sigma_s$, where $\beta\sigma_s \equiv \gamma_1 - v_0$, as a function of $X \equiv nu_0$ for fixed $h_1 = -h_2$ and different values of n (Fig. 5). As Fig. 5 shows, the region of validity of this scaling below the wetting temperature is not too wide as the scaling is very good for $X \in (-100, 20)$. Although the scaling has been derived for $T < T_w$ [Eq. (4.7)] it is also very good above the wetting temperature up to $X \sim -100$.

For the antisymmetric case of $h_1 = -h_2$ we have found an asymptotic divergence with the size of the strip M, of the two largest eigenvalues below the wetting temperature; this leads to exponential divergence with M of the correlation length $\xi_\parallel$:

$$\xi_\parallel \sim A(T, h_1) \exp(M/(u_0^{-1})) \tag{6.2}$$

valid for $M \gg u_0^{-1}$. This behavior is associated with the nearly broken symmetry of having the interface bound to the wall $(-)$ or to wall $(+)$.[6,16]

In the second case $h_1 h_2 < 0$ and $|h_1| \neq |h_2|$, we have obtained that the correlation length at low temperatures in the nonwet regime depends on the relative value of the surface fields h_1 and h_2 but is almost (up to the exponentially small corrections) *independent* of the width M of the strip [see (4.21)]. This corresponds to the system in which the predominant configurations are those with an interface bound to the wall energetically preferred, effectively those of a semi-infinite system.

Above the wetting temperature, for both cases we find the soft-mode with known properties[12,16,20,23] very little affected by the values of surface fields. We find the same finite-size dependence [Eq. (4.15)] as for the planar fluctuating interface in the capillary-wave dominant regime, even though it was derived[20] (see also Refs. 12 and 16) for $(+/-)$ strips with no weakening of bonds ($a_1 = a_2 = 1$ yielding $T_w = 0$).

For a different derivation of the asymptotic behavior of the correlation length, from the two-point bond-energy correlation function, see Ref. 7.

For the case of perfect asymmetry we have derived analytically the finite-size scaling function [see (4.14)] for $\xi_\parallel$ near the bulk wetting transition. We have also calculated numerically $\xi_\parallel$ and plotted $\ln(\xi_\parallel/n^2)$ as a function of $X \equiv nu_0$ for fixed $h_1 = -h_2$ and different values of n (Fig. 1). Figure 1 shows an excellent scaling for $X \in (-100, 50)$. As for the surface tension, we have obtained the scaling function only below the wetting temperature (the solid line in Fig. 1) but the scaling is valid also above $T_w(h_1)$ when the scaling function becomes a constant independent of X. The heat capacity shows less clearly the interference of wetting with the ordinary bulk phase transition between $(+)$ phase and $(-)$ phase.

We have derived formulas for the average magnetization $\langle\sigma_m\rangle$ at any point m of the strip. Formal expressions for $\langle\sigma_m\rangle$ depend on the relative signs of the surface fields. We have concentrated on systems with surface fields of opposite signs. After transforming these expressions into a form suitable for practical computations, we have calculated numerically magnetization profiles $m(z)$ for various sizes of the strip ($n \in [9, 201]$) and for various values of surface fields, $[a_1, a_2 \in (0, 1)]$.

For fixed value of n and a_1, a_2 the profile changes its shape with the temperature. In the case of the perfect asymmetry $h_1 = -h_2$ profiles are antisymmetric with respect to the center of the strip. At low temperatures the average magnetization is almost zero for all points of the strip; this corresponds to the average of two situations with the interface bound to either wall (1) or wall (2). A dramatic change in the profiles occurs when the symmetry of the system is broken by setting $a_2 = a_1 + \epsilon$ to have the interface bound to the wall (1), or setting $a_2 = a_1 - \epsilon$ to have the interface bound to the wall (2). Figure 9 shows $m(z)$ for the interface bound to the wall (1). For clarity of the figure we have not shown the other profiles with $a_2 < a_1$ as they have exactly the same shape, only the interface is located at the wall (2). These profiles are nonmonotonic near the walls at low temperatures, a feature never obtained with the SOS models.

For the perfect asymmetry the system shows strong interface fluctuations at the wetting temperature, which causes the profile to be a straight line across the whole strip, with the slope equal to 2. Such a result has been obtained in the restricted solid-on-solid model (RSOS), for strip geometry and contact surface fields.[26]

If $|h_1| \neq |h_2|$ the profiles at the wetting temperature are not linear across the whole strip. If there is a little (ϵ) difference between the surface fields, the profiles are linear in the vicinity of both walls. If $|h_2|$ is much greater than $|h_1|$ the profile is linear only near wall (1).

The single soft-mode phase profile does not depend on the relative value of the surface fields and perfectly agrees with the one obtained in the RSOS model [Eq. (5.42)]. The magnetization profiles can be usefully compared with those in $d=3$ obtained by Binder, Landau, and Ferrenberg[17] by Monte Carlo simulations. Qualitatively, there is a surprising similarity with those Monte Carlo profiles obtained with perfect antisymmetry broken by the bulk external field. We have also proposed and tested the scaling law for $m(z)$ [Eq. (5.41)].

In conclusion, we have confirmed by exact calculations all the predictions,[16] some obtained with heuristic arguments, about the unusual behavior of the antisymmetric system with surface fields of opposite signs—and found behavior of this system with symmetry broken by a slight difference in the strength of surface fields.

ACKNOWLEDGMENTS

We acknowledge a discussion with A. Ciach and several discussions with R. Evans (Bristol) and A. Parry (London). Our work has been partially supported by KBN Grant No. 2P03B01810.

[1] B. M. McCoy and T. T. Wu, *The Two-Dimensional Ising Model* (Harvard University Press, Cambridge, MA, 1973); B. McCoy, in *Phase Transition and Critical Phenomena*, edited by C. Domb and J. L. Lebowitz (Academic, London, 1972).

[2] H. N. V. Temperley, in *Phase Transition and Critical Phenomena*, edited by C. Domb and J.L. Lebowitz (Academic, London, 1972), Vol. 1; C. D. Domb, in *ibid*., Vol. 3.

[3] R. J. Baxter, *Exactly Solved Models in Statistical Mechanics* (Academic, London, 1982).

[4] D. B. Abraham, in *Phase Transition and Critical Phenomena*, edited by C. Domb and J. L. Lebowitz (Academic, London, 1986), and references therein.

[5] M. E. Fisher and H. Au-Yang, Physica (Utrecht) **101**, 255 (1980); H.Au-Yang and M.E. Fisher, Phys. Rev. B **21** 3956 (1980).

[6] V. Privman and M. E. Fisher, J. Stat. Phys. **33**, 385 (1983).

[7] D. B. Abraham, N. M. S̃vrakic̃, and P.J. Upton, Phys. Rev. Lett. **68**, 423 (1992).

[8] B. Kaufman, Phys. Rev. **76**, 1232 (1949); T. D. Schultz, D. C. Mattis, and E. H. Lieb, Rev. Mod. Phys. **36**, 856 (1964).

[9] D. B. Abraham, Stud. Appl. Math. **L**, 71 (1971).

[10] D. B. Abraham and A. Martin-Löf, Commun. Math. Phys. **32**, 245 (1973).

[11] D.B. Abraham and P. Reed, Commun. Math. Phys. **39**, 35 (1976).

[12] J. Stecki, A. Maciolek, and K. Olausen, Phys. Rev. B **49**, 1092 (1994).

[13] For a review, see R. Evans, J. Phys. Condens. Matter **2**, 8989 (1990).

[14] M. E. Fisher and H. Nakanishi, J. Chem. Phys. **75**, 5837 (1981); H. Nakanishi and M. E. Fisher, *ibid*. **78**, 3279 (1983).

[15] F. Brochard-Wyart and P. G. de Gennes, C. R. Acad. Sci. **297**, II 223 (1983).

[16] A. O. Parry and R. Evans, Physica A **181**, 250 (1992); see also Phys. Rev. Lett. **64**, 439 (1990).

[17] K. Binder, D. P. Landau, and A. M. Ferrenberg, Phys. Rev. Lett. **74**, 298 (1995); Phys. Rev. E **74**, 298 (1995), and references therein.

[18] M. R. Swift, A. L. Owczarek, and J. O. Indekeu, Europhys. Lett. **14**, 475 (1991); J. O. Indekeu, A. L. Owczarek, and M. R. Swift, Phys. Rev. Lett. **66**, 2174 (1991).

[19] D. B. Abraham, Phys. Rev. Lett. **44**, 1165 (1980).

[20] D. B. Abraham and N. M. Švrakić, Phys. Rev. Lett. **56**, 1172 (1986).

[21] D. B. Abraham, Physica A **177**, 421 (1991).

[22] J. Stecki, Phys. Rev. B **47**, 7519 (1993).

[23] R. Evans and J. Stecki, Phys. Rev. B **49**, 8842 (1984).

[24] L. Onsager, Phys. Rev. **65**, 117 (1944).

[25] A. Maciolek, Ph.D. thesis, Institute of Physical Chemistry of the Polish Academy of Science, Warsaw, 1995; J. Phys. A (to be published).

[26] A. Ciach and J. Stecki, J. Phys. A **20**, 5619 (1987); see also A. O. Parry, R. Evans, and D. B. Nicolaides, Phys. Rev. Lett. **67**, 2978 (1991).